Dynamic analysis of
Soil-Foundation Interaction

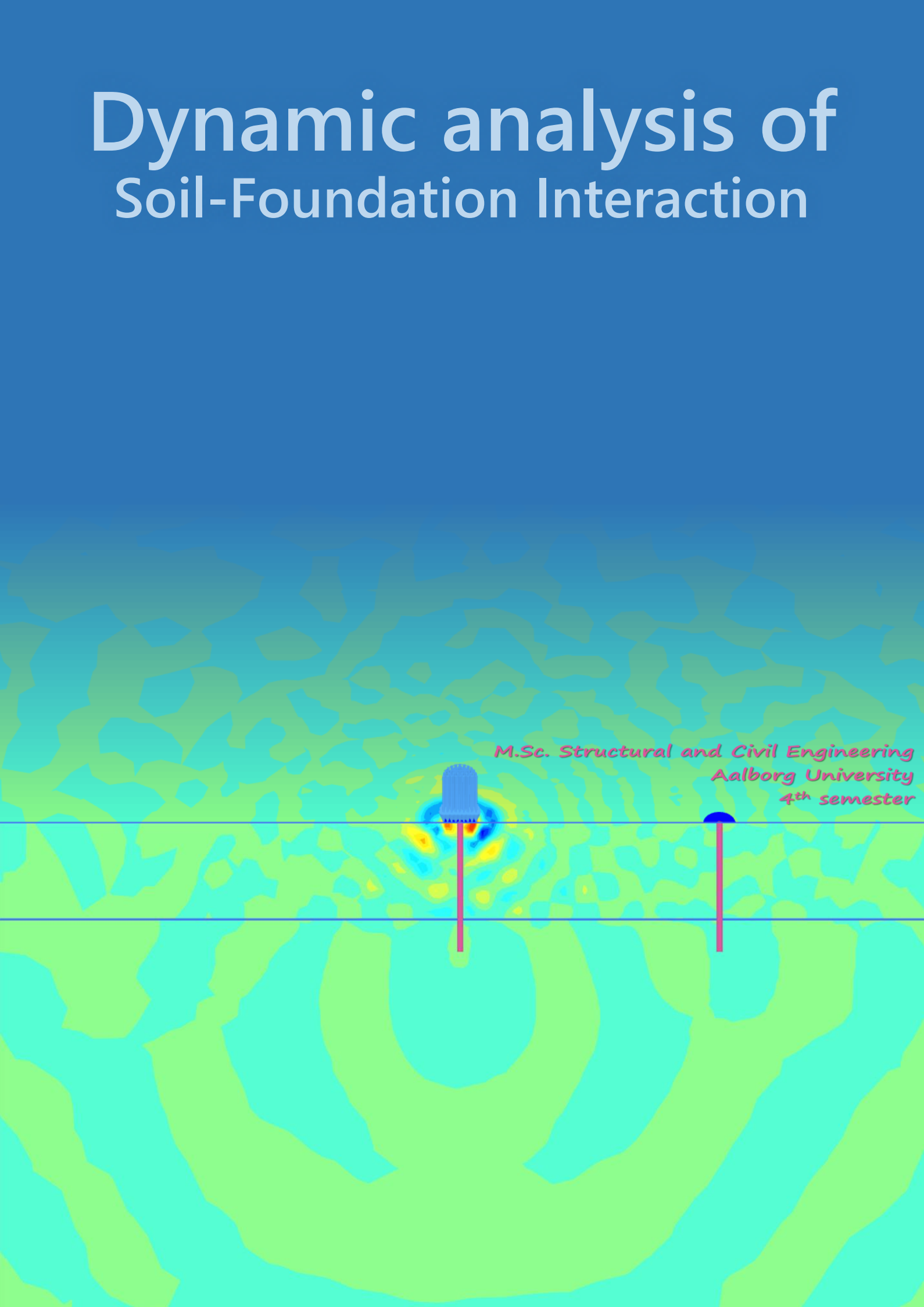

M.Sc. Structural and Civil Engineering
Aalborg University
4th semester

AALBORG UNIVERSITY
STUDENT REPORT

The faculty of Engineering and Science
Department of Civil Engineering
Sofiendalsvej 9-11, 9200 Aalborg SV
Telephone: 99 40 84 84
http://www.civil.aau.dk

Title:
Dynamic analysis of Soil-Foundation Interaction

Project period:
M.Sc., 4th semester Spring 2016

Participant:

Joeri N. Prins

Supervisor:
Lars V. Andersen

Circulation: 3
Number of pages: 89
Number of appendixes: 2
Closed the: June 3, 2016

Synopsis:

This project consists of a dynamic analysis of Soil-Foundation Interaction, i.e. Soil-Structure Interaction (SSI) and Structure-Soil-Structure Interaction (SSSI). The aim of the project is to study different wave propagation patterns. This has been studied in time domain. The used frequencies will be representative for man-made environmental vibrations. Firstly, the basic theory is explained and based on this theory, a simple model is described for surface waves. Secondly, the finite element model is described and based on both models, a comparison between the methods is made. After all basic properties and assumptions, the actual patterns in the soil is studied in time domain. Different parameters are analysed and their respective influence on the results is explained. The last part of this project contains the SSI, wherein different foundation configurations are excited with pulse and harmonic loads and the vertical responses at another foundation, some distance away, are analysed. This results in a suggestion for simplification of the model.

AALBORG UNIVERSITET
STUDENTERRAPPORT

Det Teknisk-Naturvidenskabelige Fakultet
Institut for Byggeri og Anlæg
Sofiendalsvej 9-11, 9200 Aalborg SV
Telephone: 99 40 84 84
http://www.byggeri.aau.dk

Titel:
Dynamisk analyse af Jord-Fundament Interaktion

Projektperiode:
M.Sc., 10th semester Forår 2016

Deltager:
Joeri N. Prins

Vejleder:
Lars V. Andersen

Oplagstal: 3
Sidetal: 89
Antal bilag: 2
Afleveringsdato: 3 juni 2016

Synopsis:

Dette projekt består af en dynamisk analyse af Jord-Fundament Interaktion, dvs. Jord-Struktur-Interaktion (JSI) og Struktur-Jord-Struktur Interaktion (SJSI). Formålet med projektet er at studere forskellige bølge udbredelses mønstre. Dette er blevet undersøgt i tids domæne. De anvendte frekvenser repræsenterer menneskeskabte, miljømæssige vibrationer. Først, er det grundlæggende teori forklaret og baseret på denne teori, er en simpel model for overflade bølger beskrevet. Dernæst, er finite element metoden beskrevet, hvorefter disse modeller er sammenlignet med hinanden. Efter der er redegjort for grundlæggende egenskaber og antagelser, er de faktiske mønstre på jordoverfladen undersøgt i tids domæne. Forskellige parametre er analyseret og deres respektive indflydelse på resultatet er forklaret. Den sidste del af rapporten fokuserer på JSI, hvor fundamentet er påvirket med forskellige konfigurationer af puls og harmonisk belastning og det vertikale respons af dette er analyseret i en afstand, ved et andet fundament. Dette resulterer i et forslag om at simplificere modellen.

Preface

This project contains a master thesis, called "Dynamic analysis of Soil-Foundation Interaction." written by student in the 4^{th} semester of the M.Sc. in Structural and Civil Engineering at the Faculty of Engineering and Science at Aalborg University. The project was conducted from 25 January 2016 till 3 June 2016. The aim of the project is to perform a dynamic analysis of soil-foundation interaction. This project is divided in a basic knowledge part, a parameter study and the actual soil-foundation interaction study. The final model results has been partly published as, Appendix A, "Influence of foundation type and soil stratification on ground vibration - A parameter study". For the understanding of this project, knowledge of dynamics, finite element model and geotechnical engineering are required.

Reading guide

This project contains a main report and appendices. The main report contains the basics, assumptions, method and reflection. The appendix contains the published paper (Internoise Paper), which is based on this project. As external appendix, the required PLAXIS log files to recreate the data are attached where possible. The total library of PLAXIS data is over 300 Gb, thus the appendix will include instructions for PLAXIS to recreate the data files. Also the MATLAB files are included in this external appendix. The Harvard method is used for source references. The book reference is indicated by author, year of publication, ISBN-number, edition and publisher. Tables, equations and figures are numbered in accordance with each chapter and sections, if they are without a reference to a source, it has been made by myself. Websites are indicated by title, author, URL and date of download. All the sources have been collected in a bibliography in an alphabetical order.

Acknowledgements

The author would like to show its gratitude to Lars Andersen for his guidance during this project.

Contents

Chapter 1

Introduction

It is expected that world's urban population is growing in the following years. Most of this growth is expected in the developing countries, mainly Africa and Asia as seen in Figure 1.1. The more populated urban area might result in a heavier used infrastructure by vehicles or a more dense built area in the cities.

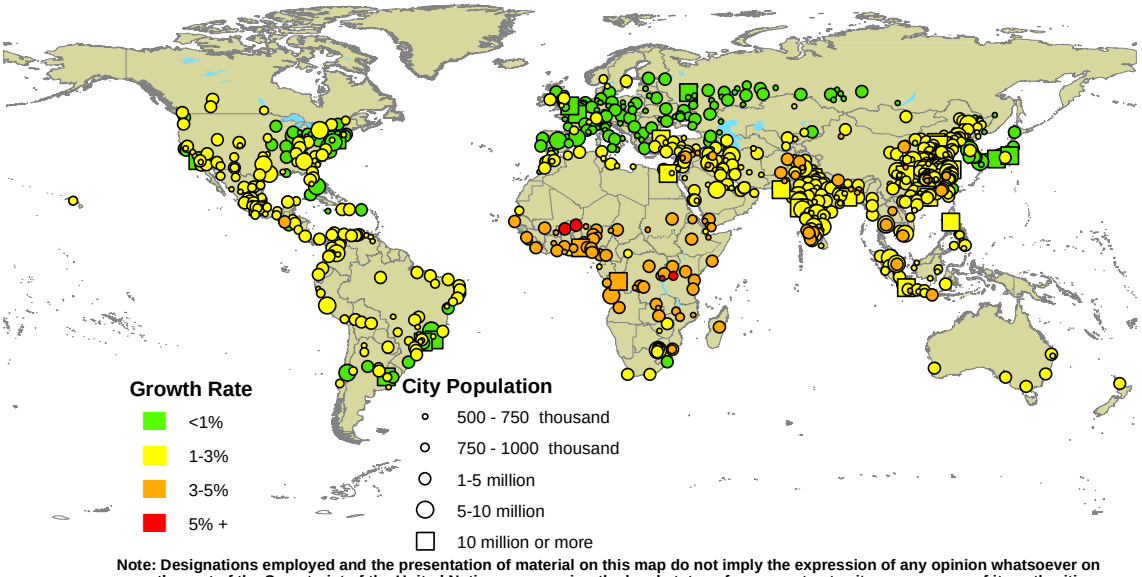

Figure 1.1: Population growth in urban areas worldwide [United Nations, Department of Economic and Social Affairs, 2015].

Movement of vehicles generates a dynamic load on the topsoil. These dynamic loads cause waves in the soil. Every type of vehicle has its own load and frequency on which waves propagate. These frequency specific waves influence the surrounding soil. In the surrounding soil, the waves will propagate with a speed specified by the soil properties.

Similar to traffic, machinery or people can produce dynamic loads and waves in a built environment, which will propagate throughout the structure of the building to the surrounding soil [Sahar & Narayan, 2016]. Both traffic and machinery waves can be described as man-made vibrations. Figure 1.2 illustrates waves in the soil from different sources.

Every type of structure in the surrounding area can be build on shallow footings or deep

foundations depending on the subsoil conditions. The man-made vibration-induced wave which is spread through the soil will influence these type of foundations. How this wave will propagate and reach a structure is complex to calculate.

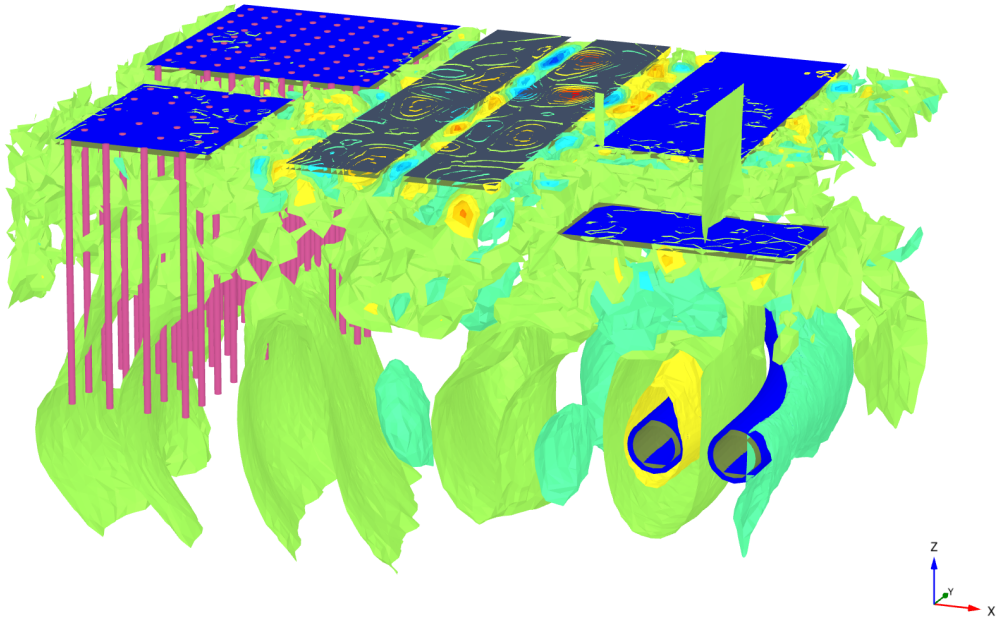

Figure 1.2: Environmental man-made vibrations in soils.

In this thesis, the wave-induced problem is simplified to an equivalent finite-element model. A three-dimensional numerical model will be used for an appropriate estimation of the soil behaviour. This model will be verified with theories known for wave propagation. Subsequently parameters that might influence the result are determined. The aim of this project is to investigate different wave propagation patterns for slab and pile foundations and to further discuss the possibility of simplifying the calculations.

Chapter 2

Wave propagation

Vibrations happens in every type of elastic medium. These vibrations will propagate through the soil in a specific wave pattern. This chapter will explain the basic theory of wave propagation through the soil. Firstly, the basics of the governing equations are explained in the equation of motions section. Secondly, this theory is used to describe the body waves, surface waves, interface waves and the one-dimensional wave. Subsequently a comparison is made between the different type of waves. And finally, refraction and reflection is introduced for layered soils.

A wave propagates through every medium. These waves are generated by a specific source. The source for elastic media can be an earthquake or so-called man-made vibration. In both cases the propagation of waves from the source shows a similar behaviour, as illustrated in Figure 2.1. These waves or vibrations have influence on structures and people. At low frequencies it might be felt by people [Plagenhoef, 1992] or it can hit the eigen frequency of a structure [Lombaert & Degrande, 1999].

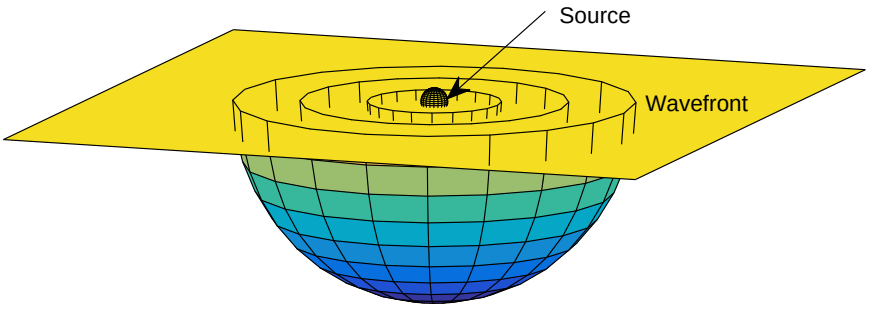

Figure 2.1: Theoretical wave propagation.

Figure 2.1 illustrates mainly the behaviour of body waves in homogeneous soils. This is the main assumption in the theory, described in this chapter. Some waves only exist in layered soils, such as the Love wave. Thus, where required, this theory is extended to layered soils. In addition, layered soils might introduce other behaviour of waves due to reflection and refraction.

2.1 Equations of motion

In the previous part theoretical wave fronts are showed. These wave fronts are based on the theory related to the equation of motions. These equations are described further in this section.

The equations of motion describes the behaviour of a system as function of time and spatial coordinates. In this project it is used to describe the wave propagation.

For the formulation of the equations of motion in an infinite linear-elastic domain is established. Within this domain an infinitesimal cube with $\mathrm{d}x \cdot \mathrm{d}y \cdot \mathrm{d}z$ as dimensions exists, illustrated in Figure 2.2. The cubic is homogeneity, which implies the elasticity modulus E and the mass density ρ are independent on position.

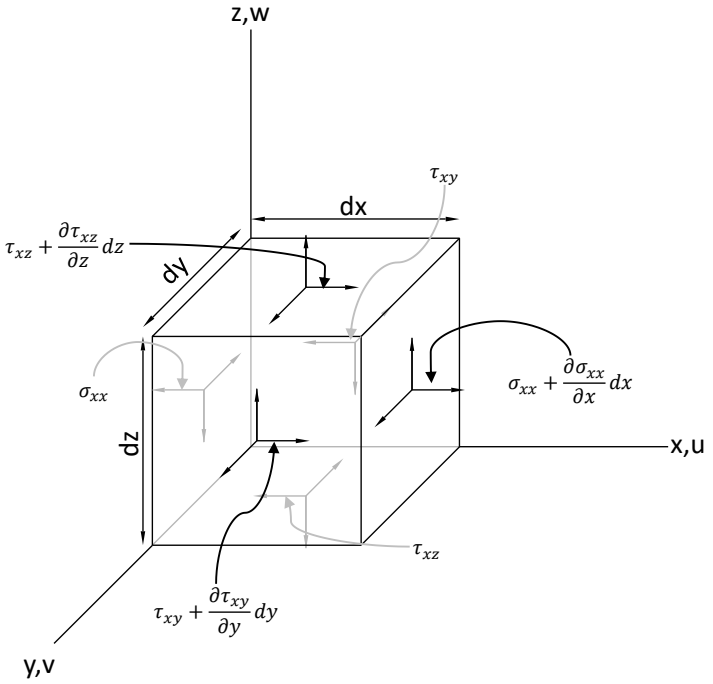

Figure 2.2: Stresses in the x-direction on an infinitesimal cube.

There are two types of motion; kinematics and dynamics. In the following solution of the equation, dynamic motion is used, which takes into account force, momentum and particle acceleration. The used differential equation is Newton's second law of motion. Newton's second law describes

$$\vec{F} = m\vec{a}, \tag{2.1}$$

with $\vec{F}$ as force vector, m as mass and $\vec{a}$ as acceleration vector.

Newton's second law is only valid for a constant mass. Due to change of spacial coordinates,

the mass does not change. Applying Newton's second law on the cube in x-direction illustrated in Figure 2.2, and applying a body force b that acts on the mass $\rho \cdot (\mathrm{d}x \cdot \mathrm{d}y \cdot \mathrm{d}z)$, the equilibrium equation

$$\begin{aligned}
&\left(\sigma_{xx} + \frac{\partial \sigma_{xx}}{\partial x}\mathrm{d}x\right) \cdot \mathrm{d}y \cdot \mathrm{d}z - \sigma_{xx} \cdot \mathrm{d}y \cdot \mathrm{d}z \\
&+ \left(\tau_{xy} + \frac{\partial \tau_{xy}}{\partial y}\mathrm{d}y\right) \cdot \mathrm{d}x \cdot \mathrm{d}z - \tau_{xy} \cdot \mathrm{d}x \cdot \mathrm{d}z \\
&+ \left(\tau_{xz} + \frac{\partial \tau_{xz}}{\partial z}\mathrm{d}z\right) \cdot \mathrm{d}x \cdot \mathrm{d}y - \tau_{xz} \cdot \mathrm{d}x \cdot \mathrm{d}y \\
&+ \rho b_x \cdot (\mathrm{d}x \cdot \mathrm{d}y \cdot \mathrm{d}z) = \rho \cdot (\mathrm{d}x \cdot \mathrm{d}y \cdot \mathrm{d}z) \cdot \frac{\partial^2 u}{\partial t^2},
\end{aligned} \tag{2.2}$$

can be obtained. A similar expression can be made for directions y and z. With manipulating the equation and rewriting it in index notation it becomes

$$\rho \ddot{u}_i = \sigma_{ij,j} + \rho b_i. \tag{2.3}$$

By assuming the material as Linear-Elastic, the stresses can be expressed as strains based on Hooke's law

$$\sigma_{ij} = E_{ijkl}\epsilon_{kl}, \tag{2.4}$$

where E_{ijkl} is the elasticity tensor and ϵ_{kl} a strain tensor. The elasticity tensor is symmetric. This equation is known as the physical condition. The geometrical condition is the relation between strains and displacement, when assuming small deformations it is known as

$$\epsilon_{ij} = \frac{1}{2}\left(u_{i,j} + u_{j,i}\right). \tag{2.5}$$

When the stress-strain relationship assumed to be isotropic, Equation 2.4 can be further simplified to [Andersen, 2006]

$$\sigma_{ij} = \lambda u_{k,k}\delta_{ij} + 2\mu\epsilon_{ij}, \tag{2.6}$$

with λ and μ as Lamé constants, related to Young's modulus E and Poisson ratio ν

$$\begin{aligned}
\lambda &= \frac{\nu E}{(1+\nu)(1-2\nu)}, \\
\mu &= \frac{E}{2(1+\nu)},
\end{aligned} \tag{2.7}$$

and δ_{ij} as Kronecker delta,

$$\delta_{ij} = \begin{cases} 1 & \text{for } i = j \\ 0 & \text{for } i \neq j. \end{cases} \tag{2.8}$$

By substituting all known conditions in Equation 2.3, it can be rewritten to obtain the

strong form, also known as Navier equations;

$$\rho\ddot{u}_i = (\lambda + \mu)\, u_{j,ij} + \mu u_{i,jj} + \rho b_i. \tag{2.9}$$

From Navier equations, the elastic wave propagation in terms of velocity can be expressed. This process is explained in following section.

2.2 Body waves

In an elastic soil are two different waves propagating. These waves are dilatational and rotational waves. The first wave or primary wave (P-wave) is a dilatational wave. This wave is obtained by differentiating Equation 2.9, so that

$$\rho\frac{\partial^2\epsilon}{\partial t^2} = (\lambda + \mu)\,\nabla^2\epsilon + \mu\nabla^2\epsilon, \tag{2.10}$$

and wherein ϵ is the divergence of the the displacement vector

$$\epsilon = u_{k,k} \tag{2.11}$$

and the Laplace operator ∇ is

$$\nabla^2 = \frac{\partial^2}{\partial x^2} + \frac{\partial^2}{\partial y^2} + \frac{\partial^2}{\partial z^2}, \tag{2.12}$$

and with rearranging Equation 2.10 to

$$\frac{\partial^2\epsilon}{\partial t^2} = V_p^2\nabla^2\epsilon, \tag{2.13}$$

the variable V_p is introduced as the phase velocity of the first wave, showed in

$$V_p = \sqrt{\frac{\lambda + 2\mu}{\rho}}. \tag{2.14}$$

The secondary wave (S-wave) is a rotational wave, based Equation 2.9, the secondary wave is obtained by applying the curl on the displacement vector, so that

$$\rho\frac{\partial^2\Omega_i}{\partial t^2} = \mu\nabla^2\Omega_i, \tag{2.15}$$

and wherein the curl is defined as

$$\Omega_i = \frac{1}{2}\left(\epsilon_{ijk}\frac{1}{2}\left(u_{j,k} - u_{k,j}\right)\right), \tag{2.16}$$

similar to the P-wave, Equation 2.15 can be rearranged and wherein the shear wave phase velocity V_s denotes

$$V_s = \sqrt{\frac{\mu}{\rho}}. \tag{2.17}$$

2.3 Surface waves

In previous section the body waves are explained. Figure 2.3 illustrates the propagation direction of two wave types, the Rayleigh wave and the Love wave. Firstly the Rayleigh wave is explained and afterwards the Love wave.

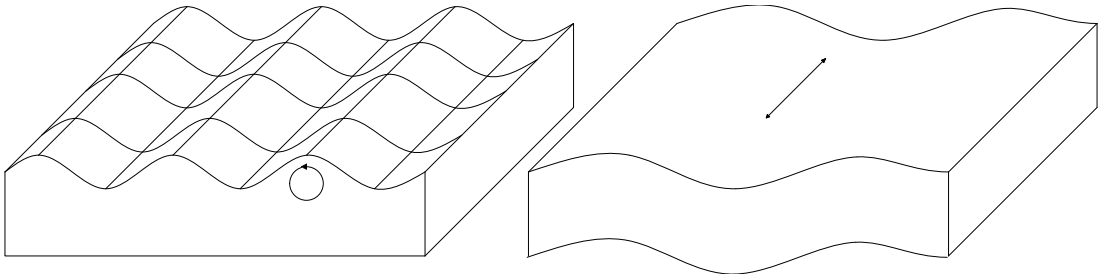

Figure 2.3: Propagation direction of Rayleigh and Love wave.

On free surface, there is a possibility of mixing two body waves (P- and S-wave). This wave is described as a Rayleigh wave. The Rayleigh wave travels in a semi-infinite body, where the particle velocity of the wave close to the surface is relatively high compared to particle velocity further away from the surface [Pichugin, 2008].

Lord Rayleigh described the velocity in the equation

$$\left(2 - V_r^2\right)^2 = 4\sqrt{1 - V_r^2}\sqrt{1 - \chi V_r^2}, \tag{2.18}$$

wherein V_r is described as the Rayleigh wave phase velocity and the non-dimensional χ is defined as

$$\chi = \frac{V_s^2}{V_p^2}. \tag{2.19}$$

With rearranging this equation, the Rayleigh wave is expressed with

$$K_{rs} = \frac{V_r}{V_s}, \tag{2.20}$$

as parameter of the secondary wave V_s:

$$K_{rs}^6 - 8K_{rs}^4 + \left(24 - 16\chi^2\right) K_{rs}^2 + 16\left(\chi^2 - 1\right) = 0. \tag{2.21}$$

K_{rs} is a factor what has in Equation 2.21 six non-zero roots. However, only one of these

roots is valid. For the Poisson ratio interval $\nu \in [0,0.5]$, a real material, only one root is real and acceptable, which is lower than $K_{rs} < 1.0$, since the Rayleigh wave phase velocity is lower than the S-wave phase velocity.

With knowing the Rayleigh wave phase velocity, the velocity is used to describe the particle motion of the soil. A Rayleigh wave propagates on a two dimensional plane with a phase velocity V_r and in the x-direction [Heaton, 2005]. When assuming an elastic half-space, the motion equations can be considered as

$$\begin{aligned} u_x &= \mathbb{R}\left(A \exp\left(-bz\right) \exp\left[ik_r\left(x - V_r t\right)\right]\right), \\ u_y &= 0, \\ u_z &= \mathbb{R}\left(B \exp\left(-bz\right) \exp\left[ik_r\left(x - V_r t\right)\right]\right), \end{aligned} \tag{2.22}$$

where $\mathbb{R}$ denotes the real part of the complex number, k_r the Rayleigh wave number, and the real part b, which is positive. A solution to this real part is expressed as

$$\left[V_p^2 b^2 - \left(V_p^2 - V_r^2\right) k_r^2\right] \left[V_s^2 b^2 - \left(V_s^2 - V_r^2\right) k_r^2\right] = 0. \tag{2.23}$$

The constants A and B can be obtained by the ratios correspond to the roots of b. Where,

$$b_1 = k_r \left(\frac{V_r^2}{V_p^2}\right)^4, \quad b_2 = k_r \left(\frac{V_r^2}{V_s^2}\right)^4, \tag{2.24}$$

and the ratio is defined as

$$\frac{B}{A} = -\frac{b_1}{ik_r}, \quad \frac{B}{A} = \frac{ik_r}{b_2}. \tag{2.25}$$

By applying the constants, Equation 2.22 yields

$$\begin{aligned} u_x &= Ck_r \left(\exp\left(-qz\right) - \frac{2qs}{s^2 + k_r^2} \exp\left(-sz\right)\right) \sin\left(\omega t - k_r x\right), \\ u_z &= Cq \left(\exp\left(-qz\right) - \frac{2k_r^2}{s^2 + k_r^2} \exp\left(-sz\right)\right) \sin\left(\omega t - k_r x\right), \end{aligned} \tag{2.26}$$

where C is height of surface at $x = 0, t = 0$, ω is the angular frequency, and q and s are factors, depending on

$$\begin{aligned} \frac{q^2}{k_r^2} &= 1 - \chi^{-2} K_{rs}^2, \\ \frac{s^2}{k_r^2} &= 1 - K_{rs}^2. \end{aligned} \tag{2.27}$$

Rayleigh waves can originate from two different sources, a line source and a point source. At a line source, plane Rayleigh waves exists, where it from a point source circular spread from its origin. With the equation above, it is assumed that the wave propagates continuously at the same amplitude. Due to the geometrical spreading of the wave, the amplitude of

the wave decrease exponentially with $1/\sqrt{r}$, where r is the radius from the source point. This is illustrated in Figure 2.4, wherein Equation 2.26 is solved.

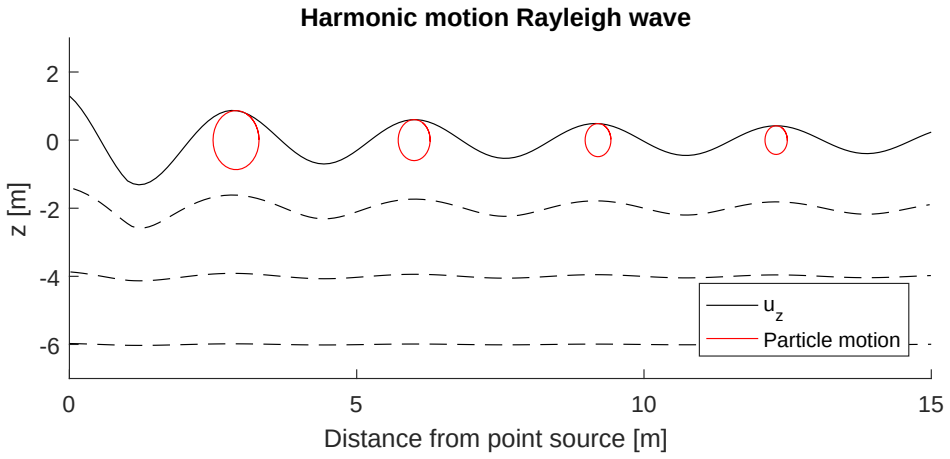

Figure 2.4: Theoretical surface motion of Rayleigh wave.

Figure 2.4 shows the particle path of the harmonic Rayleigh wave in homogeneous soil. The particle motion at free surface is an ellipse, with the vertical component about 1.5 times the horizontal amplitude. The horizontal particle motion is $\pi/2$ out of phase from the vertical component. Rayleigh waves can be observed in both vertical and radial components on a seismograph. A characteristic Rayleigh wave is known as retrograde particle motions, the particles are moving counter clockwise for a wave propagating towards the right. At greater depths, the particle motion is reversed, i.e. prograde.

Waves propagating in traverse direction might occur in layered soils. This traverse wave is called the Love wave. A Love wave only occurs in the surface layer when the soil is less stiff compared to the underlying half-space below

$$\frac{G_1}{\rho_1} \ll \frac{G_2}{\rho_2}, \tag{2.28}$$

where G_1 is the shear modulus of the top layer, and G_2 of the underlying layer. ρ_1 denotes the mass density of the top layer, and ρ_2 for the bottom. The phase velocity V_l is frequency depended and can be expressed as

$$\tan \omega H \left(\frac{1}{V_{s;1}^2} - \frac{1}{V_l^2} \right)^{\frac{1}{2}} = \frac{G_2}{G_1} \frac{\sqrt{\frac{1}{V_l^2} - \frac{1}{V_{s;2}^2}}}{\sqrt{\frac{1}{V_{s;1}^2} - \frac{1}{V_l^2}}}, \tag{2.29}$$

where H denotes the soil layer depth and $V_{s;1}$ the S-wave phase velocity for the top layer and $V_{s;2}$ for the underlying. The particle motion of a Love wave in x-direction was described

by Love [1929] as

$$u_y = \left\{ A_1 \exp\left[-k_l z \sqrt{1 - \frac{V_l^2}{V_{s;1}^2}} \right] + A_1' \exp\left[kz \sqrt{1 - \frac{V_l^2}{V_{s;1}^2}} \right] \right\} \exp\left[i \left(k_l x - \omega t \right) \right], \quad (2.30)$$

in the top layer and

$$u_y = A_2 \exp\left[-k_l z \sqrt{1 - \frac{V_l^2}{V_{s;2}^2}} \right] \exp\left[i \left(k_l x - \omega t \right) \right], \quad (2.31)$$

in the layer below. The love wave should satisfy Navier equations Equation 2.9 (p. 8), motion u_y which is continues at $z = 0$, the stress σ_{yz} which is continues as $z = 0$, and $\sigma_{yz} = 0$ at $z = -H$. The constants A_1, A_1' (top layer) and A_2 (underlying layer) can be solved by applying these boundary conditions.

The phase velocity of a low frequency Love wave tends to be similar to the high-velocity half space. Whereas high frequency waves are vice versa. A Love wave might be generated at a point source. If this happens, the waves are observed as transverse waves in the component of motions. These type of waves have their motion at the surface and spreads circularly from the point of origin. The amplitude decay with the same ratio as the Rayleigh wave, $1/\sqrt{r}$.

2.4 Interface waves

In addition to the body waves and surface waves, waves at a certain boundary might occur too. These waves are called the Stonely and Scholte wave. In this section, both wave types are shortly explained.

The wave existing along a solid-solid interface is called a Stonely wave. A Stonely wave can be measured by the displacement of an interface [Flores-Mendez et al., 2012]. The energy in the wave decays away from the interface. The Stonely wave is a complex wave to define. This wave is related to the primary and secondary wave in both solids existing at the interface [Achenbach, 1973]. The velocity proportional to the secondary wave speed can be obtained by

$$\alpha^2 \left[1 - \left(\frac{\alpha K_{ss}}{\kappa_2} \right)^2 \right]^{\frac{1}{2}} R_1 + \left[1 - \left(\frac{K_{ss}}{\kappa_1} \right)^2 \right]^{\frac{1}{2}} \frac{\mu_2}{\mu_1} R_2 = 0, \quad (2.32)$$

wherein the relations between the secondary wave α and relation between primary and

secondary wave κ are expressed as

$$\begin{aligned} \alpha &= \frac{V_s}{V_p}, \\ \kappa &= \frac{V_p}{V_s}, \end{aligned} \tag{2.33}$$

and the parameters R_1 and R_2 as

$$\begin{aligned} R_1 &= \left(2 - K_{ss}^2\right)^2 - 4\left[1 - \left(\frac{K_{ss}}{\kappa}\right)^2\right]^{\frac{1}{2}} \left(1 - K_{ss}^2\right)^{\frac{1}{2}}, \\ R_2 &= \left(2 - \alpha^2 K_{ss}^2\right)^2 - 4\left[1 - \left(\frac{\alpha K_{ss}}{\kappa_2}\right)^2\right]^{\frac{1}{2}} \left(1 - \alpha^2 K_{ss}^2\right)^{\frac{1}{2}}, \end{aligned} \tag{2.34}$$

these equations can be solved to obtain K_{ss}, which is defined as the Stonely wave phase velocity V_d proportional to the S-wave velocity of the top layer:

$$K_{ss} = \frac{V_d}{V_s}. \tag{2.35}$$

A wave propagating at a fluid-soil interface is called a Scholte wave. Scholte waves have a wide range of applications and may exist in every type of fluid. The Scholte wave is based on a range of experiments of the interaction between an inviscid fluid and an elastic solid. According to Vinh [2013], the Scholte wave is related to the body wave velocities and the properties of the fluid. The phase velocity is obtained by the following equation:

$$\frac{\rho^*}{\rho} K_{fs}^2 \sqrt{1 - \chi K_{fs}} + \left(2 - K_{fs}\right)^2 \sqrt{1 - \chi^* K_{fs}} - 4\sqrt{1 - K_{fs}}\sqrt{1 - \chi K_{fs}}\sqrt{1 - \chi^* K_{fs}} = 0, \tag{2.36}$$

where χ is the dimensionless relation between the primary and shear wave speed, $\chi*$ the relation of the shear wave compared to the primary wave in the fluid, ρ is mass density of the soil, ρ^* mass density of the fluid and K_{fs} is the dimensionless velocity of the Scholte wave as function of the S-wave speed

$$K_{fs} = \frac{V_f^2}{V_s^2}. \tag{2.37}$$

2.5 1D bar wave

Pile foundations are often dimensioned as a one-dimensional (1D) beams. The theory for this wave uses Equation 2.3 (p. 7), but only for one direction, in this case the x-direction.

Using a linear relationship, the elasticity modulus becomes

$$E = \frac{\sigma}{\epsilon}, \tag{2.38}$$

and with substituting this equation in Equation 2.3 and Equation 2.5 (p. 7) it is expressed as

$$\begin{aligned} \rho \ddot{u}_k &= E u_{k,kk}, \\ \ddot{u}_k &= V_b^2 u_{k,kk}, \end{aligned} \tag{2.39}$$

where the 1D bar phase velocity V_b denotes

$$V_b = \sqrt{\frac{E}{\rho}}. \tag{2.40}$$

2.6 Comparison of wave types

Four types of waves are discussed in previous sections; body waves, surface waves, interface waves and the one-dimensional wave. The different types of waves are related to each other with a certain factor. This factor varies along the interval of $\nu \in [0,0.5]$, which is also illustrated in Figure 2.5.

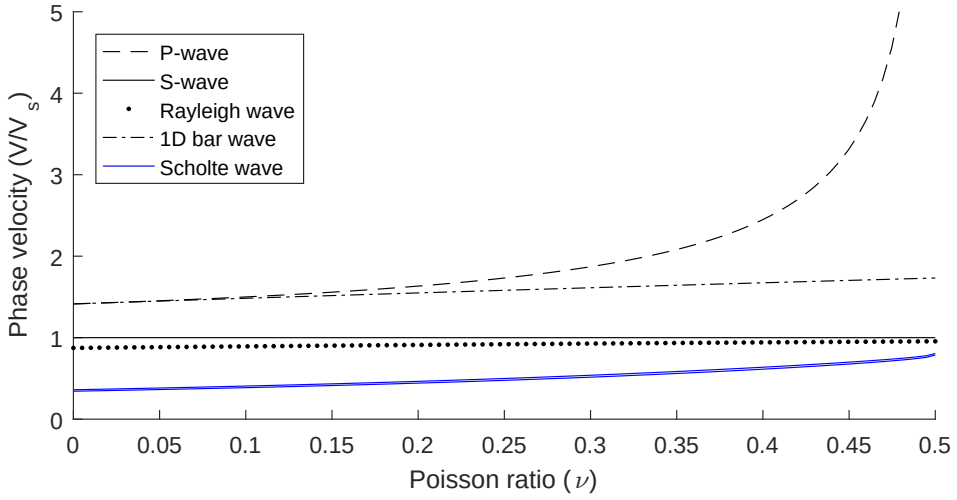

Figure 2.5: Relative propagation speed in terms of V_s as function of Poisson ratio ν.

Figure 2.5 describes the relation proportional to the shear wave velocity. This S-wave velocity can be measured in a laboratory and thus all other interesting wave speeds are known from this graph. For the Scholte wave, the graph differs between different densities of fluids and thus this solution needs to be checked in different situations. However, both

fresh water and salty water are added into the figure, what results in a slightly different value ($\approx 5\%$ offset). The Love and Stonely wave are not included in this graph. This is since those waves are depending on the difference in material properties between the two layers at the interface.

For further investigation of dynamic soil-foundation interaction, this basic theory of waves is used in deriving governing equations of the finite element method. In homogeneous soils, the main interest is based on the Rayleigh wave. When observing results in layered media, a combination of several wave types might occur, due to reflection and refraction at interfaces between different material densities, which is further explained in next section.

2.7 Layered soils

In previous part, the theory is explained as infinite homogeneous medium. In reality soil is bounded to possible inhomogeneous medium. When a wave, which propagates with a certain speed, hits a boundary, the wave might reflect or get transmitted. In a one dimensional case this is explained as [Andersen, 2006]

$$u^i(0,t) + u^r(0,t) = u^t(0,t), \tag{2.41}$$

where u is the particle displacement divided into u^i incoming, u^r reflected and u^t transmitted particle displacement.

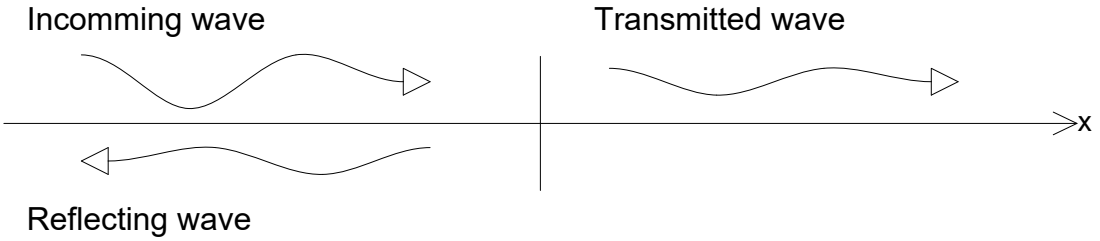

Figure 2.6: Basic theory reflecting and transmitted wave.

Based on Figure 2.6 and Equation 2.41, it can be mentioned that the velocity and stresses should be equal on both sides, since the energy is fully transmitted or reflected. Thus, the following relation can be made

$$\sigma^i(0,t) + \sigma^r(0,t) = \sigma^t(0,t), \tag{2.42}$$

where σ is wave stress. Since the wave is propagating in positive x-direction, $\sigma(0,t) = zv(t)$, whereas negative x-direction implies $\sigma(0,t) = -zv(t)$. This results in

$$z_1 v^i(t) + z_1 v^r(t) = z_2 v^t(t), \tag{2.43}$$

with v denoting the particle velocity, respective for v^i incoming, v^r reflected and v^t transmitted waves. And z as material impedance, i.e. $z_k = \rho_k V_k$, based on the mass density ρ and the phase velocity V. Combining both equations, two additional parameters can be obtained as reflection C_r and transmission C_t coefficients

$$\begin{aligned} C_r &= \frac{v^r(t)}{v^i(t)}, \\ C_t &= \frac{v^t(t)}{v^i(t)}, \end{aligned} \tag{2.44}$$

and can be used to obtain an impedance mismatch. This impedance mismatch describes the relation between two different soils. A range of transmission and reflection coefficients based on impedance mismatch is illustrated in Figure 2.7. As the impedance mismatch is getting greater, a wave gets fully reflected and not transmitted.

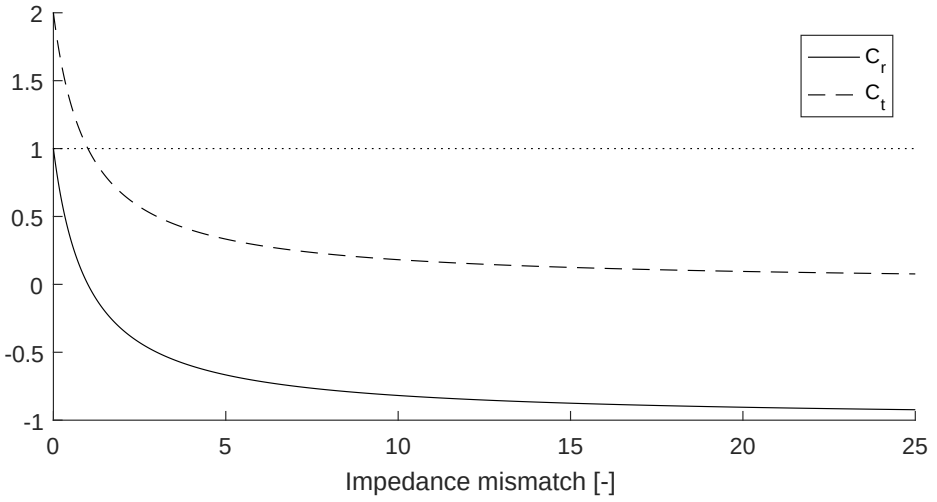

Figure 2.7: Coefficients in relation to impedance mismatch.

The solution above explains an one dimensional case, only this report uses three dimensional models, thus this theory will be slightly modified. An example is provided in Figure 2.8, wherein a wave is not perpendicular to a boundary. In this situation the incoming wave triggers reflected and refracted waves.

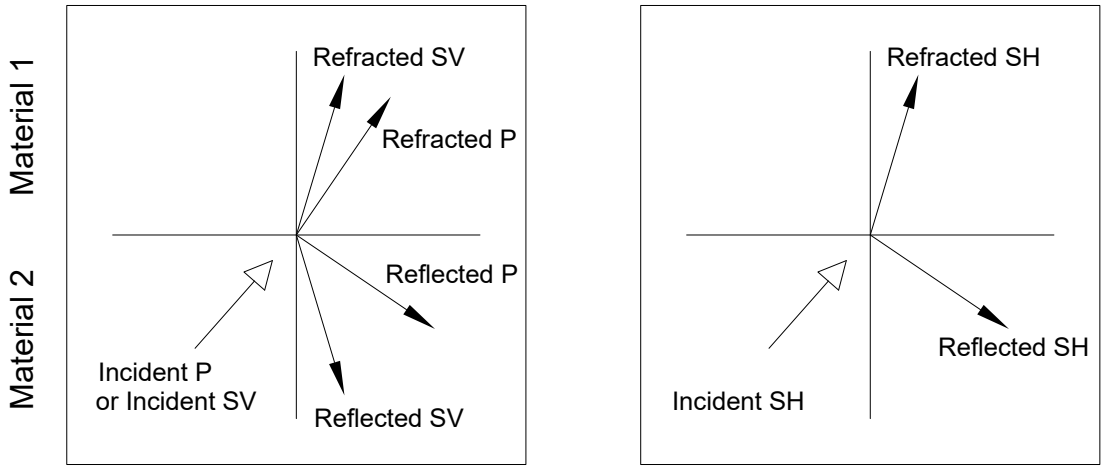

Figure 2.8: Reflection and refraction of body waves.

The ratio of waves which are transmitted can be obtained by Snell's law [Ni et al., 2011]. Snell's law describes the relation between angle of incident θ_1 related to angle of refraction θ_2 with respect to the phase velocity of the different materials V_1 and V_2

$$\alpha = \frac{V_1}{V_2} = \frac{\sin\theta_1}{\sin\theta_2}. \tag{2.45}$$

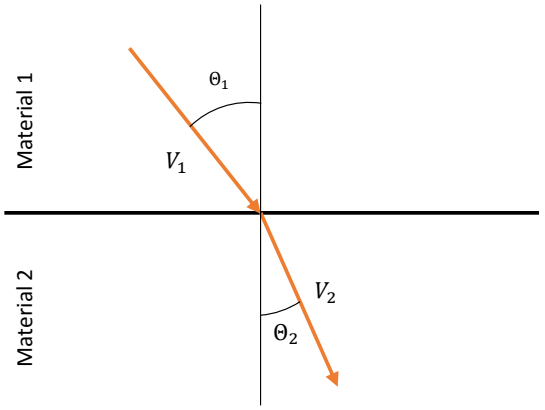

Figure 2.9: Principle of Snell's law.

Chapter 3

Soil-Pile interaction

The interaction between soil and piles is a complicated problem and has been researched by many through the years. A more complicated situation occurs during vibration. Since the pile interacts with both the surrounding soil and the soil on the end of the pile. The dynamic soil-pile interaction is studied and explained in several models, such as the dynamic Winkler model and several three-dimensional continuum models. Within next section some obtained results of these models relevant to this project are explained.

3.1 Previous studies

Much studies uses the dynamic Winkler model. A model which explains the behaviour of soil near a pile foundation. Based on the model proposed by Nogami & Novák [1976], Yu et al. [2013] has studied the effect of sediments on bedrock. The pile is considered rock-socketed, and the study focusses on vertical dynamic impedance at the head of the pile. The increase of sediment, i.e. layer thickness, leads to significant influence on the vertical impedance at the pile head. It was observed that the ability of a pile to resist dynamic vertical deformation was weakened. However, resistance was increased with the increase of S-wave velocity.

Deng et al. [2014] uses this theory but instead of using a single impulsive force, a harmonic force is introduced. In this study, the interacting soil is assumed to be viscoelastic material and the governing equations are subjected to arbitrary harmonic dynamic force, based on Bernoulli-Euler rod theory. Finally, a relation of the parameters of the pile end soil is studied. A main statement is made that the pile end soil layer adjacent to the pile end has significant influence on the dynamic response at the pile head and the influence of the thickness is critical. A note to this study is that the decrease of the pile length and increase of the pile radius might be more remarkable at the pile head.

Padrón et al. [2012] describes a method for superposition pile groups versus slab footings, with the use of a three-dimensional frequency domain elastodynamic BEM-FEM formulation. It implements an elastodynamic analyses of piled embedded footings. The main overview is that vertical responses decreases faster with piles by frequency than without piles. But in overall the response of embedded footings provides a suitable estimate of the piled behaviour.

Cai et al. [2000] proposed with his study a three-dimensional finite element subsystem methodology with an advanced plasticity-based constitutive model for soils. It combines different methods for frame elements and solid elements. In this approach, cyclic behaviour of soft clays and tangent matrices of soil properties are formulated separately and coupled due to kinematic interaction. This method requires time domain seismic input, although it has a limitation in multiple structures, and thus, this method can only be used for simple structures. Furthermore, this theory focus on soil near foundation.

From this point of view, the interest remains with the main question, what will happen at a certain distance from the pile, especially with layered soils, since most studies found relations at or near the pile surface. For the use of this type of analysis, a finite element solver may be used, which is in a certain situations a valid solution.

3.2 Finite element model

For the numerical analysis, the finite element is used. In this section the theory behind the finite element is explained for this particular case. For this finite element model, the following basic assumptions were made:

- The surrounding soil is isotropic and viscoelastic and can be extended towards infinity, the domain boundaries are viscous.
- There is no displacement occurring at the bottom of the domain.
- Dynamic motion is considered, static response due to gravity is neglected.

3.2.1 Strong and weak form

In order to perform a finite element analysis, the first step is establishing a partial differential equation, the strong form [Cook et al., 2007].

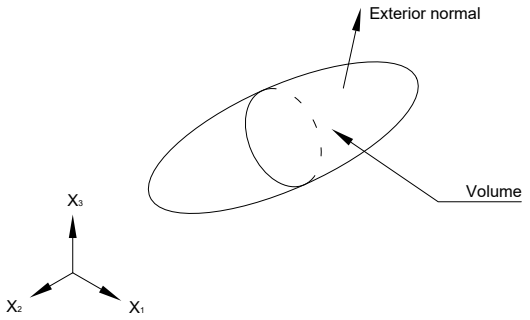

Figure 3.1: Arbitrary body with volume Ω and surface S.

The strong from consists of a traction vector $\boldsymbol{t}$ and a boundary normal vector $\boldsymbol{n}$. The relation is as follow

$$t_i = \sigma_{ij} n_j. \tag{3.1}$$

Based on the strong form, expressed in Equation 2.9 (p. 8) the equation can be rewritten with the use of Gauss' divergence theorem, wherein it is depending on the volume

$$\int_\Omega (b_i + \sigma_{ij,j} - \rho \ddot{u}_i)\, \mathrm{d}\Omega = 0. \tag{3.2}$$

The strong form is multiplied with a weight function δu(x,y,z) and integrate it over its domain

$$\int_\Omega \delta u_i b_i \mathrm{d}\Omega + \int_\Omega \delta u_i \sigma_{ij,j} \mathrm{d}\Omega - \int_\Omega \delta u_i \rho \ddot{u}_i \mathrm{d}\Omega = 0, \tag{3.3}$$

with using the Green-Gauss theorem, the following expression is obtained

$$\int_\Omega \delta u_i b_i \mathrm{d}\Omega + \oint_S \delta u_i t_i \mathrm{d}S - \int_\Omega \delta u_{i,j} \sigma_{ij} \mathrm{d}\Omega - \int_\Omega \delta u_i \rho \ddot{u}_i \mathrm{d}\Omega = 0. \tag{3.4}$$

This can be rewritten in matrix notation, and thus the weak form results in

$$\int_\Omega (\tilde{\nabla} \boldsymbol{U})^T \sigma \mathrm{d}\Omega + \int_\Omega \boldsymbol{U}^T \rho \ddot{\boldsymbol{u}} \mathrm{d}\Omega = \oint_S \boldsymbol{U}^T \mathbf{t} \mathrm{d}S + \int_\Omega \boldsymbol{U}^T \mathbf{b} \mathrm{d}\Omega, \tag{3.5}$$

which contains the following vectors

$$\boldsymbol{u} = \begin{Bmatrix} u_x \\ u_y \\ u_z \end{Bmatrix}, \boldsymbol{b} = \begin{Bmatrix} b_x \\ b_y \\ b_z \end{Bmatrix}, \boldsymbol{U} = \begin{Bmatrix} \delta u_x \\ \delta u_y \\ \delta u_z \end{Bmatrix}, \tilde{\nabla} \boldsymbol{U} = \begin{Bmatrix} \frac{\partial \delta u_x}{\partial_x} \\ \frac{\partial \delta u_y}{\partial_y} \\ \frac{\partial \delta u_z}{\partial_z} \\ \frac{\partial \delta u_x}{\partial_y} + \frac{\partial \delta u_y}{\partial_x} \\ \frac{\partial \delta u_y}{\partial_z} + \frac{\partial \delta u_z}{\partial_y} \\ \frac{\partial \delta u_x}{\partial_z} + \frac{\partial \delta u_z}{\partial_x} \end{Bmatrix}. \tag{3.6}$$

3.2.2 Shape-, Weight Functions and Stiffness Matrix

Different materials have their own respective shape and weight functions. However, not every structural element has the same element. For example, when introducing a pile foundation, two different methods can be used:

- Pile foundation assumed as solid (solid-solid model).
- Foundation assumed as embedded beam (beam-solid model).

In all situations both methods are available, only a pile or beam is usually modelled as 1D

structural element or 2D shell element, since 3D solid element requires more computational effort.

To use computational power more efficiently, several mesh types are combined. For the soil a tetrahedron mesh is used with 10 nodes, the slab foundation uses a quadratic triangular element (LST, 6 nodes) on top of the soil and for the pile a 3 node beam element penetrating the soil is used. This beam element can be embedded in a solid element, i.e. crossing a 10-node tetrahedron in any arbitrary direction [Brinkgreve et al., 2015a].

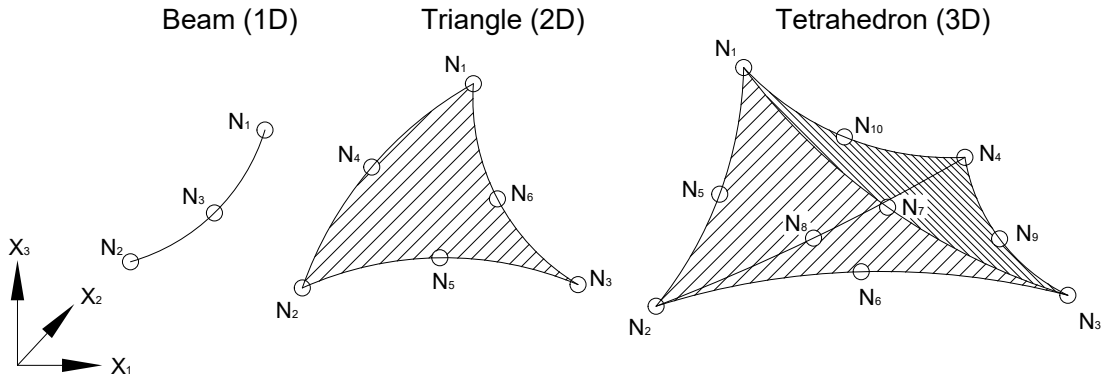

Figure 3.2: Different types of elements used.

According to Galerkin's method, each point is determined relatively to the values of the element when deformation happens. The determination can be obtained by interpolation. Shape functions are used to carry out interpolation between the nodes of an element. The displacement within an element can be described as $u(x,y,z) = \mathbf{N}\boldsymbol{U}$. Wherein the vector $\boldsymbol{U}$ contains the displacements of a node within the element

$$\boldsymbol{U} = \begin{Bmatrix} U_x^1 & U_y^1 & U_z^1 & \cdots & U_x^n & U_y^n & U_z^n \end{Bmatrix}^T, \tag{3.7}$$

and $\mathbf{N}$ is a matrix containing the shape functions

$$\mathbf{N} = \begin{bmatrix} N^1 & 0 & 0 & \dots & N^n & 0 & 0 \\ 0 & N^1 & 0 & \dots & 0 & N^n & 0 \\ 0 & 0 & N^1 & \dots & 0 & 0 & N^n \end{bmatrix}, \tag{3.8}$$

wherein n is the number of nodes within an element. The shape functions for a 3 node beam element are

$$N^1 = -\tfrac{1}{2}(1-\xi)\xi \quad N^2 = \tfrac{1}{2}(1+\xi)\xi \quad N^3 = (1+\xi)(1-\xi), \tag{3.9}$$

the 6 node triangular element

$$\begin{aligned} N^1 = \zeta\,(2\zeta - 1) \quad N^2 = \xi\,(2\xi - 1) \quad N^3 = \eta\,(2\eta - 1) \\ N^4 = 4\zeta\xi \qquad N^5 = 4\xi\eta \qquad N^6 = 4\eta\zeta, \end{aligned} \tag{3.10}$$

with ζ used as auxiliary coordinate, i.e. $\zeta = 1 - \xi - \eta$. A 10 node tetrahedron element consists of the following shape functions

$$\begin{aligned} N^1 = (1-\xi-\eta\zeta)(1-2\xi-2\eta-2\zeta) \qquad N^2 = \zeta(2\zeta-1) \qquad N^3 = \xi(2\xi-1) \\ N^4 = \eta(2\eta-1) \qquad N^5 = 4\zeta(1-\xi-\eta-\zeta) \qquad N^6 = 4\xi\zeta \\ N^7 = 4\xi(1-\xi-\eta-\zeta) \qquad N^8 = 4\eta(1-\xi-\eta-\zeta) \qquad N^9 = 4\eta\zeta \\ N^{10} = 4\xi\eta. \end{aligned} \tag{3.11}$$

For the stiffness matrix, the strain interpolation matrix is used $\epsilon(x,y,z) = \tilde{\nabla}\mathbf{N}\boldsymbol{U} = \mathbf{B}\boldsymbol{U}$. This strain interpolation matrix is described as

$$\mathbf{B} = \begin{bmatrix} \frac{dN^1}{dx} & 0 & 0 & \dots & \frac{dN^n}{dx} & 0 & 0 \\ 0 & \frac{dN^1}{dy} & 0 & \dots & 0 & \frac{dN^n}{dy} & 0 \\ 0 & 0 & \frac{dN^1}{dz} & \dots & 0 & 0 & \frac{dN^n}{dz} \\ \frac{dN^1}{dy} & \frac{dN^1}{dx} & 0 & \dots & \frac{dN^n}{dy} & \frac{dN^n}{dx} & 0 \\ 0 & \frac{dN^1}{dz} & \frac{dN^1}{dy} & \dots & 0 & \frac{dN^n}{dz} & \frac{dN^n}{dy} \\ \frac{dN^1}{dz} & 0 & \frac{dN^1}{dx} & \dots & \frac{dN^n}{dz} & 0 & \frac{dN^n}{dx} \end{bmatrix}. \tag{3.12}$$

Within the element, the derivation between local and global coordinates involves the Jacobian $\mathbf{J}$:

$$\begin{bmatrix} \frac{\partial N^n}{\partial \xi} \\ \frac{\partial N^n}{\partial \eta} \\ \frac{\partial N^n}{\partial \zeta} \end{bmatrix} = \mathbf{J} \begin{bmatrix} \frac{\partial N^n}{\partial x} \\ \frac{\partial N^n}{\partial y} \\ \frac{\partial N^n}{\partial z} \end{bmatrix}. \tag{3.13}$$

The stress-strain relationship $\sigma = \mathbf{D}\epsilon$ can be expressed with use of the flexibility matrix

$$\mathbf{D} = \frac{E}{(1+\nu)(1-2\nu)} \begin{bmatrix} 1-\nu & \nu & \nu & & & \\ \nu & 1-\nu & \nu & & 0 & \\ \nu & \nu & 1-\nu & & & \\ & & & \frac{1-2\nu}{2} & & \\ & 0 & & & \frac{1-2\nu}{2} & \\ & & & & & \frac{1-2\nu}{2} \end{bmatrix}. \tag{3.14}$$

Finally, the stiffness matrix can be obtained from

$$\mathbf{K}^e = \int_{\Omega_e} \mathbf{B}^T \mathbf{D} \mathbf{B} \mathrm{d}\Omega_e, \tag{3.15}$$

since the integrand varies over the element, numerical integration according to the Gauss rule is recommended [Felippa, 2004]:

$$\begin{aligned} \mathbf{K}^e &= \int_\zeta \int_\eta \int_\xi \mathbf{B}^T \mathbf{D} \mathbf{B} \mathrm{d}\xi \mathrm{d}\eta \mathrm{d}\zeta, \\ \mathbf{K}^e_{ij} &\approx \sum_k \mathbf{B}_i^T \mathbf{D} \mathbf{B}_j \det \mathbf{J} w_k, \end{aligned} \tag{3.16}$$

wherein w_k a weight function from the Gaussian interpolation function.

3.2.3 Soil-structure connection

The structures and the soil are only connected in the global stiffness matrix. The structural elements, slab foundation and pile foundation are coupled with a rigid interface. The structure (slab and pile foundation) and soil interface is considered as spring, this is modelled as an extra thin layer around the nodes which interfere each other [Ports & Zdravkovic, 2001]. The two nodes are at the same position, but connected by a spring, the principle is illustrated in Figure 3.3.

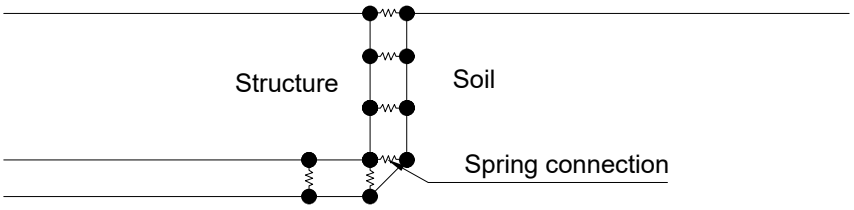

Figure 3.3: Soil-structure connection.

Interaction of a spring connection is based on a three-node line element, which will couple the nodes [Brinkgreve et al., 2015b]. The interaction is represented as skin traction $\boldsymbol{t}$, where the incremental process can be expressed as

$$\boldsymbol{t}^s = \boldsymbol{t}_0^s + \Delta \boldsymbol{t}^s, \tag{3.17}$$

where $\boldsymbol{t}_0^s$ is the initial skin traction, and $\Delta \boldsymbol{t}^s$ is the incremental skin traction. The relation

is obtained by

$$\begin{aligned}\Delta \boldsymbol{t}^s &= \mathbf{T}^s \Delta \boldsymbol{u}_{rel},\\ \Delta \boldsymbol{t}^s &= \mathbf{T}^s \left(\Delta \boldsymbol{u}_p - \Delta \boldsymbol{u}_s\right),\\ \Delta \boldsymbol{t}^s &= \mathbf{T}^s \left(\mathbf{N}_p \Delta \boldsymbol{v}_p - \mathbf{N}_s \Delta \boldsymbol{v}_s\right),\end{aligned} \tag{3.18}$$

where $\mathbf{T}^s$ denotes the material stiffness, $\mathbf{N}_p$ and $\mathbf{N}_s$ are matrices containing the shape functions of respectively a structure and soil, $\Delta \boldsymbol{u}_{rel}$ describes the incremental relative particle displacement, and $\boldsymbol{v}_p$ is the particle velocity of the structure and $\boldsymbol{v}_s$ of the soil. Using the virtual work priciple, the equations was discretised and described by Brinkgreve et al. [2015b] as

$$\int_S \delta \boldsymbol{u}_{rel}^T \Delta \boldsymbol{t}^s \mathrm{d}S = \delta \boldsymbol{v}_{rel}^T \int_S \mathbf{N}_{rel}^T \mathbf{T}^s \mathbf{N}_{rel} \mathrm{d}S \Delta \boldsymbol{v}_{rel} = \mathbf{K}^s \Delta \boldsymbol{v}_{rel}, \tag{3.19}$$

where

$$\Delta \boldsymbol{v}_{rel} = \begin{Bmatrix} \Delta \boldsymbol{v}_p & \Delta \boldsymbol{v}_s \end{Bmatrix}^T, \tag{3.20}$$

and

$$\mathbf{N}_{rel} = \begin{bmatrix} \mathbf{N}_p & -\mathbf{N}_s \end{bmatrix}. \tag{3.21}$$

The stiffness matrix $\mathbf{K}^s$ is obtained which contains the nodes that represents the interaction between the elements. This stiffness matrix is expressed as

$$\mathbf{K}^s = \begin{bmatrix} \int_S \mathbf{N}_p^T \mathbf{T}^s \mathbf{N}_p \mathrm{d}S & -\int_S \mathbf{N}_p^T \mathbf{T}^s \mathbf{N}_s \mathrm{d}S \\ -\int_S \mathbf{N}_s^T \mathbf{T}^s \mathbf{N}_p \mathrm{d}S & \int_S \mathbf{N}_s^T \mathbf{T}^s \mathbf{N}_s \mathrm{d}S \end{bmatrix}. \tag{3.22}$$

3.2.4 Boundaries

The finite element method allows modelling of finite domains. As mentioned in the assumptions, the soil is considered with an infinite length. There are several methods to model an artificial boundary at a certain distance, for example infinite elements, boundary elements, transmitting boundaries, perfect matching layers or the use of a buffer zone with high damping ratios.

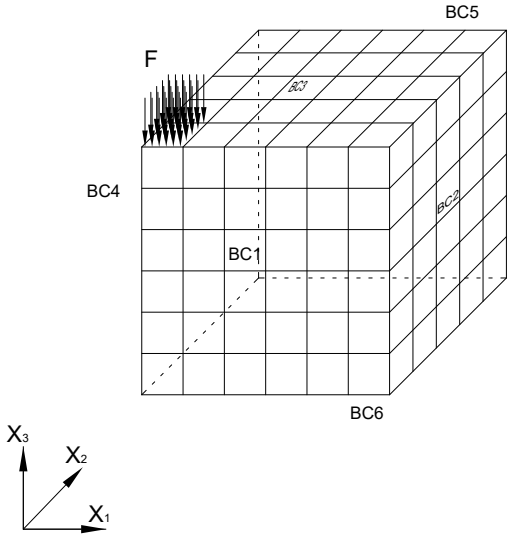

Figure 3.4: Simplified model of FE soil mesh.

Based on Figure 3.4, boundary condition 1 and 4 (BC1 and 4) are considered symmetrical, BC2 and BC5 can be extended towards infinity and results in an artificial boundary, BC3 is the free surface and BC6 is a fully fixed artificial boundary. This project uses a damper as artifical boundary, except at the free surface. These transmitting boundaries are necessary to prescribe the behaviour of an infinite soil. Waves at the boundary should be fully absorbed. The use of viscous boundaries was described by Lysmer & Kuhlemeyer [1969] as:

$$\begin{aligned} \sigma_1 &= -C_1 z_p \dot{u}_1, \\ \tau_2 &= -C_2 z_s \dot{u}_2, \\ \tau_3 &= -C_2 z_s \dot{u}_3, \end{aligned} \tag{3.23}$$

where z_p is the material impedance for the P-wave in the soil and z_p the S-wave. C_1 and C_2 are relaxation coefficients, which have been used to improve the effect of absorption. When $C_1 = C_2$, a wave hitting the boundary perpendicular gets perfectly absorbed. However, not all waves arrives perpendicular at the boundary, thus the values $C_1 = 1$ and $C_2 = 0.25$ will be used to consider a reasonable absorption. However, with this method it is not possible to fully absorb S-waves, thus, a limited boundary effect is noticeable in the obtained results.

3.2.5 Stiffness, damping and mass matrix

In previous part, the local stiffness matrix is obtained. For the overall calculations, the local stiffness matrix is transformed, with use of transformation matrix $\mathbf{T}$, to the global

coordinate system and inserted, at the right nodes, in the global stiffness matrix

$$\mathbf{K} = \mathbf{T}^T \mathbf{K}^e \mathbf{T}. \tag{3.24}$$

In general cases, the transformation matrix $\mathbf{T}$ denotes

$$\mathbf{T} = \begin{bmatrix} \mathbf{\Gamma} & & 0 \\ & \ddots & \\ 0 & & \mathbf{\Gamma} \end{bmatrix}, \tag{3.25}$$

where $\mathbf{\Gamma}$ is used for local matrix transformation within the transformation matrix. $\mathbf{\Gamma}$ yields to a matrix that rotates the axes with respect to the principle axis of the cross section (illustrated in Figure 3.5)

$$\mathbf{\Gamma} = \mathbf{\Gamma}_\alpha \mathbf{\Gamma}_\beta \mathbf{\Gamma}_\gamma. \tag{3.26}$$

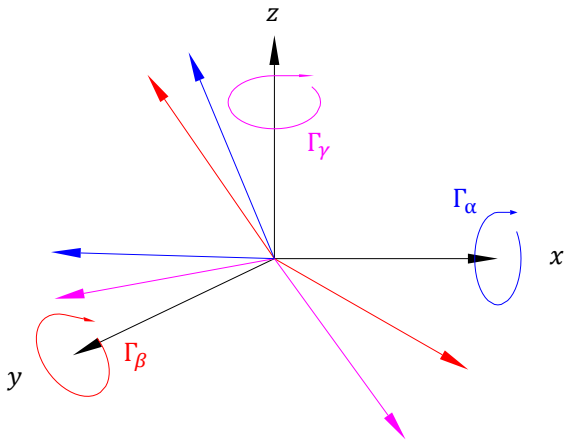

Figure 3.5: Transformation of principle axis.

In simple situations, the finite element method is described as

$$\mathbf{K}\boldsymbol{u} = \boldsymbol{F}, \tag{3.27}$$

wherein $\mathbf{K}$ is the stiffness matrix, $\boldsymbol{u}$ a displacement vector and $\boldsymbol{F}$ a vector containing external forces. This equation can be used to solve an unknown number or quantities, nodes and their respective degrees of freedom. More interest has the similar dynamic formulation, which includes inertia and damping

$$\mathbf{M}\ddot{\boldsymbol{u}} + \mathbf{C}\dot{\boldsymbol{u}} + \mathbf{K}\boldsymbol{u} = \boldsymbol{F}, \tag{3.28}$$

where $\mathbf{M}$ is the mass matrix, $\mathbf{C}$ the damping matrix, $\ddot{\boldsymbol{u}}$ acceleration vector and $\dot{\boldsymbol{u}}$ velocity vector. The damping matrix is determined by use of Rayleigh damping model, wherein

$$\mathbf{C} = \alpha_r \mathbf{M} + \beta_r \mathbf{K}. \tag{3.29}$$

The α_r and β_r are proportionality constants of the mass and stiffness matrices. α_r and β_r are calibrated with the use of two frequencies, f_1 and f_2 are chosen as the resonance frequencies related to the two first modes of a soil layer, obtained by [Kramer, 1996]:

$$f_n = V_s \frac{2n-1}{4H}, \tag{3.30}$$

with n as frequency, e.g. 1,2,... and H as depth of the soil layer. Acceptable values for damping ratio ξ are in the range [0.5%,2%], suggested by Laera & Brinkgreve [2015]. For harmonic load interaction between foundation and soils, the interest is a series of stable steady state solutions, wherein the displacement and load vectors are considered as

$$\begin{aligned} \boldsymbol{u} &= \sum_{j=1}^{N} u_j \exp\left(i\omega t\right), \\ \boldsymbol{F} &= \sum_{j=1}^{N} F_j \exp\left(i\omega t\right). \end{aligned} \tag{3.31}$$

i is considered as imaginary number $\sqrt{-1}$, ω the angular frequency and t as time. u_j and F_j are complex vectors, related to a specific frequency. The factor N is depended on frequency and soil characteristics.

3.2.6 Direct-time approach

When applying a harmonic force in time domain, Equation 3.28 is integrated by a direct time approach. For the integration the Newmark-β method is used [Newmark, 1959]. The equation of motions at time $t_{n+1} = t_n + \Delta t_n$ should be full filled

$$\mathbf{M}\ddot{u}_{n+1} + \mathbf{C}\dot{u}_{n+1} + \mathbf{K}u_{n+1} = \mathbf{F}_{n+1}, \tag{3.32}$$

with the use of predicted displacement and velocity vectors based on Taylor's theorem

$$\begin{aligned} \dot{u}_{n+1} &= \dot{u}_n + \Delta t \cdot \ddot{u}_\gamma, \\ u_{n+1} &= u_n + \Delta t \cdot \dot{u}_n + \frac{1}{2}\Delta t^2 \cdot \ddot{u}_\beta, \end{aligned} \tag{3.33}$$

in which

$$\begin{aligned} \ddot{u}_\gamma &= (1-\gamma)\ddot{u}_n + \gamma\ddot{u}_{n+1}, \\ \ddot{u}_\beta &= (1-2\beta)\ddot{u}_n + 2\beta\ddot{u}_{n+1}, \end{aligned} \tag{3.34}$$

and wherein Newmark's $\beta \leq \frac{1}{2}$ and $\gamma \leq 1$. Applying this prediction into Equation 3.32 and rearranging variables leads to

$$\mathbf{M}_d\ddot{u}_{n+1} = \mathbf{F}_{n+1} - \mathbf{C}\left(\dot{u}_n + (1-\gamma)\,\Delta t\ddot{u}_n\right) - \mathbf{K}\left(u_n + \dot{u}_n\Delta t + \left(\frac{1}{2} - \beta\right)\Delta t^2\ddot{u}_n\right), \tag{3.35}$$

with this equation, the unknown quantity $\ddot{u}_n$ is obtained by solving the following equation

$$\mathbf{M}_d = \mathbf{M} + \gamma\Delta t\mathbf{C} + \beta\Delta t^2\mathbf{K}. \tag{3.36}$$

Chapter 4

Analyses of wave theory

In Chapter 2 (p. 5), the theory of wave propagation was explained. In this chapter basic models will be described to analyse the wave propagation theory. This model uses a three dimensional finite element model. Firstly, the model properties will be described. Subsequently, the verification from the simple model will be made with other methods for calculating the same case. The proposed model consists of basic symmetric objects. In the first case a slab foundation will be excited and following up within the same domain a single pile foundation.

4.1 Model properties

In this section, the model properties will be explained. To verify the results, different analyses are performed. These models should have the same properties to obtain valid results, which can be compared in this chapter. The model is verified with the amplitude of the surface at specific distances. Important properties which should be the same through the models are Young's modulus E, Poisson ratio ν, and mass density ρ. These parameters are used to describe the Rayleigh surface wave, as stated in Section 2.3 (p. 9).

The model consists of a homogeneous layer of sand which can be extended towards infinity in horizontal and vertical direction. Damping of the material is disregarded, thus the Rayleigh coefficients α_r and β_r are equal to zero. Table 4.1 gives an outline of all material properties used for this model.

Table 4.1: Material properties of the used soil.

Soil Type	Dense sand
Material model	Linear-Elastic
Mass density ρ	$2000\,\mathrm{kg/m^3}$
Rayleigh coefficient α_r	0
Rayleigh coefficient β_r	0
Young's modulus E	50 MPa
Poisson ratio ν	0.30

In addition to material parameters the type of structure, dimensions and load is correspondingly defined through the tested models. To elucidate the soil behaviour a harmonic

force of $10\,\mathrm{kN/m^2}$ at a frequency of 5 Hz is applied on the structure. The structure consists of a squared shallow slab foundation (2-by-2 metre) and in the second case extended with a deep pile foundation, a single 8 metre long pile attached to the slab footing. The self-weight of the structure and soil is neglected in the model. The principle model is sketched in Figure 4.1.

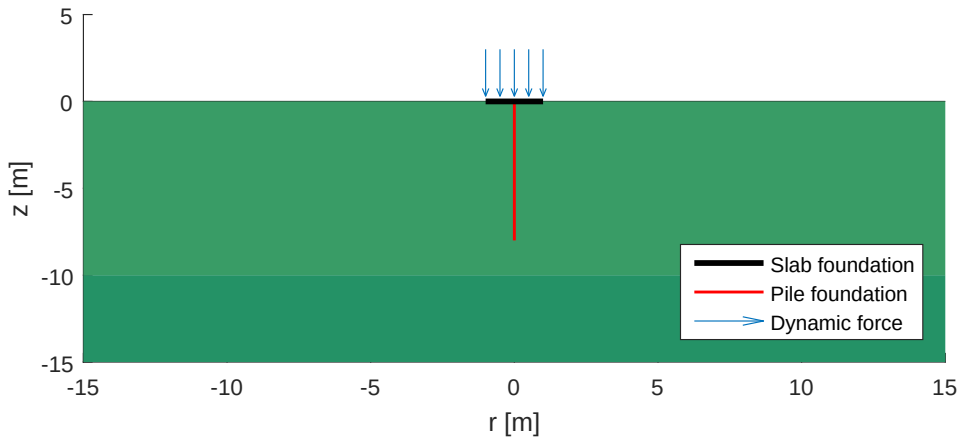

Figure 4.1: Principle model set-up.

In the finite element models, the top layer mesh is finer defined compared to the bottom ones to save computing time. By defining global parameters for this case, a likewise result can be obtained using the models described in the following section.

4.2 Tested models

To get a better understanding of soil behaviour, several programs and methods are performed with the same problem. This type of analysis is used to validate the results and determine the method which is satisfied for more advanced modelling of structures. The objective of this analysis is to determine the amplitude at different positions and compare it with other models. In this section, the methods and some required assumptions or limitations are defined.

4.2.1 PLAXIS

PLAXIS is a commercial Finite Element Method tool used for geotechnical applications. PLAXIS can be used in different type of analyses in two dimensions and three dimensions [Brinkgreve et al., 2015a]. Both versions of PLAXIS are used for simulating this problem. However, it is assumed that the PLAXIS 3D model describes the influences of the surrounding soil more accurate compared to the PLAXIS 2D model. The foundation in the 2D model has an infinite length, thus it is assumed the amplitudes are relatively higher

than the 3D model. Waves propagate in three dimensions, the interest for results of this analysis is in singular plane (e.g. $x = 0, y \in [-\infty,\infty]$ and $z \in [-\infty,0]$).

The dynamical module of PLAXIS is used. In the first basic model, a slab and pile foundation are modelled in the middle of the domain. On this structure, a harmonic dynamic force will be added at a specific frequency, as described earlier in this chapter. The soil is defined as a linear-elastic material, in which the wave propagation theory as proposed before is valid. The calculation of the dynamic force in PLAXIS is based on Newmark's-β method [Newmark, 1959]. The used coefficients of this method are based on the average acceleration ($\beta = \frac{1}{2}$ and $\gamma = \frac{1}{4}$).

4.2.2 MATLAB Analytical

Based on the theory of Section 2.3 (p. 9) an analytical model is build in MATLAB. The analytical, as simplified model, is a rough estimation of the situation of the soil. It has a limitation since it only calculates the surface amplitude with a pre described pattern of geometrical spreading. For a shallow foundation, this can give a rough estimation which could be valid. In case of the deep pile foundation, it does not take into account the wave starting from the bottom of the pile. This model is based on Equation 2.26 (p. 10), with as start amplitude the initial settlement as described by Lutenegger & Groot [1995]. For homogeneous cases the model could be valid and explaining the basic theory. When using a layered situation this model ignores positive and negative interference at a receiving point.

4.3 Comparison

In previous section, different methods to tackle a simplified foundation-soil interaction problem were introduced. These programs are performed and for each program the results at the surface are collected. Figure 4.2 illustrates those results, the figure divides the type of calculation with a particular colour. Furthermore, the shallow slab foundation is a continuous line and the deep pile foundation is a dashed line.

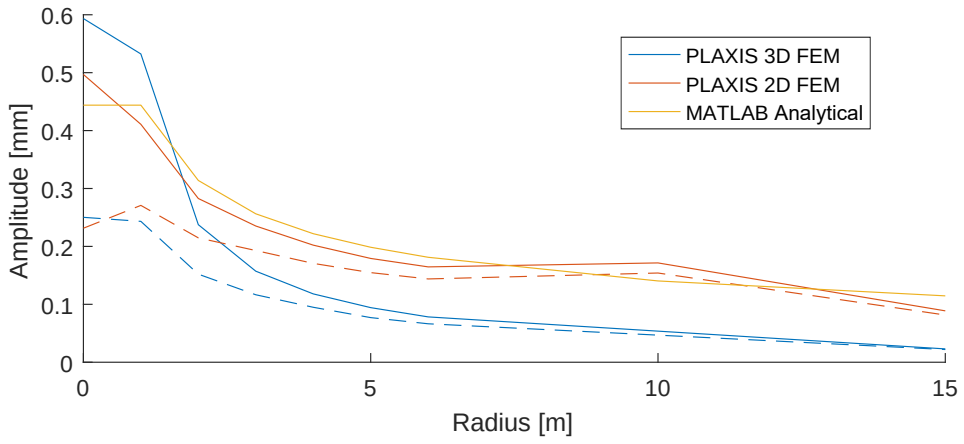

Figure 4.2: Surface amplitudes of various theories.

Based on Figure 4.2 and the wave propagation theory for homogeneous soils, the analytical solution could be used. However, the interest consists of different soil stratifications and different foundation configurations, thus, the analytical model would not be suitable. The analytical model shows a relation to the curves from the 2D FEM slab foundation, those distributions are similar to each other.

The 2D FEM illustrates a reasonable output. The influence of foundations and different soil stratifications could be modelled with this model. However, the model assumes an infinite row of foundations, thus circular geometric spreading of the Rayleigh wave is not correctly modelled. The more advanced 3D FEM follows a likewise path to both other models, thus this method is considered valid for further calculation.

Chapter 5

Parameter study

In previous chapters, the basic theory and used model is explained and validated. For continuing calculations, it is necessary to know what are the influences of different parameters in the calculation. Firstly, the model properties are explained, a small verification for correctness of the model is made and subsequently the results of this analyses are introduced. Towards the end, parameters which has significant influence on the results are obtained.

5.1 Model

For the investigation of wave propagation a three-dimensional finite element model is made. Parameters used in every single model are likewise for comparison. The model is defined as Linear-Elastic and for calculation the commercial FEM tool PLAXIS 3D was used. Properties of the soil are described in Table 5.1.

Table 5.1: Material properties of the used soil.

Soil Type	Unit	Clay	Sand
Material model		Linear-Elastic	Linear-Elastic
Mass density ρ	[kg/m^3]	1400	1700
Young's modulus E	[MPa]	20	50
Poisson ratio ν	[-]	0.25	0.30

Assumed is a domain consisting of an infinite medium in each direction. This total area is reduced to a medium described with a certain interest area. The artificial boundary distance d away from the source is related to the relative error ϵ, and was descibed by Chen et al. [2015]. The suggestion is based on the shear wavelength λ and was only examined for frequencies below 100 Hz:

$$d = \begin{cases} 0.1\lambda & \text{for } \epsilon = 6.8\% \\ 0.2\lambda & \text{for } \epsilon = 1.2\%. \end{cases} \tag{5.1}$$

To obtain valid results the mesh within this artificial boundary is more refined, and extended with a buffer area so that the model boundaries would not cause much interference in the results. Figure 5.1 illustrate the geometry in x-z plane, where H is depends on

homogeneous soils or layered soils.

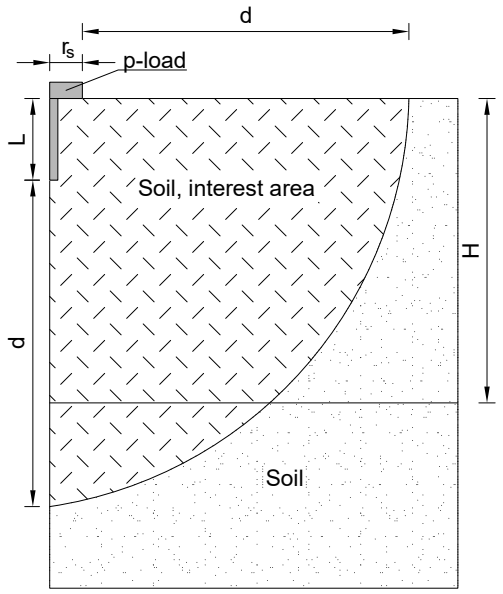

Figure 5.1: Schematic situation tested models.

The model boundary conditions are defined as viscous boundaries, excluding the surface. It is assumed that all boundaries absorbs the wave energy completely. The mesh is further refined at the interest points. The mesh consists of 10-node triangular elements, as explained earlier. These elements have a maximum dimension in which the result is suitable for further usage. Kuhlemeyer & Lysmer [1973] suggested an element size l_e in relation to the wavelength

$$l_e \leq \frac{\lambda}{8}. \tag{5.2}$$

Within the interest area, this relation is valid. Outside the interest area, i.e. the buffer zone, the element size might be larger as required, especially for higher frequencies. The mesh as generated is illustrated in Figure 5.2. Dynamic interaction between the foundation and soil is simulated by adding a slab for shallow foundations and pile for deep foundations. The pile has different sizes in the range $L_p \in [0{,}6] \cdot r_s$. A harmonic uniform surface load p is added on top of the slab. This surface force is multiplied with a sinusoidal time series multiplier with specific frequencies. The tested frequencies were representative for environmental man-made vibrations, described by Lombaert et al. [2001].

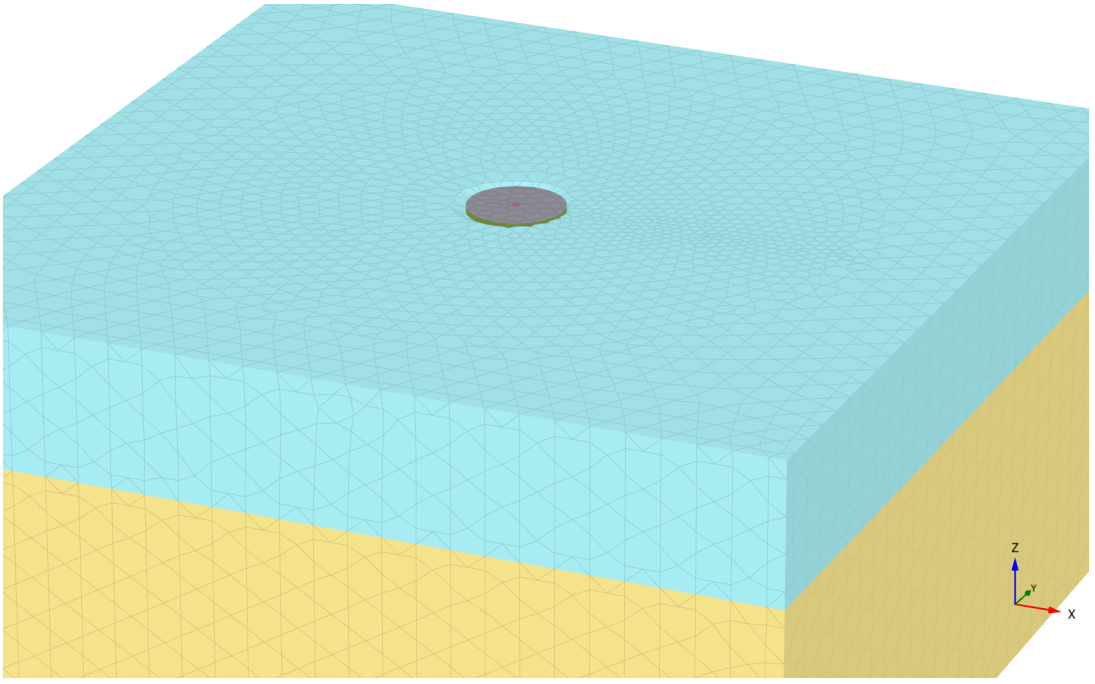

Figure 5.2: Layered soil mesh.

Dynamic equations are integrated based on steps in a time series. For these integrations Newmark-β method is used [Newmark, 1959]. The used coefficients of this method are based on the average acceleration. The calculation in PLAXIS uses sub-steps, these sub-steps are automatically generated by PLAXIS based on number of data points, material properties and time step. The model is solved over a time domain of a few seconds, which depends on the minimum time for a wave to propagate through the model in the soil

$$t_{min} = C_d \frac{d}{V_r}, \tag{5.3}$$

where d is the distance between the source foundation and a receiver point, and C_d a coefficient slightly higher than 1.0 to ensure the Rayleigh wave is received at the receiver. The amount of steps in the model is depending on the frequency, to ensure a down-crossing analysis can be performed based on the peaks in time series at different positions. The critical time step to assure no wave passes an element unnoticed is defined by Pal [1998] as:

$$\Delta t_{critical} = \frac{l_e}{\alpha_t \sqrt{\frac{E(1-\nu))}{\rho(1+\nu)(1-2\nu)}} \sqrt{1 + \frac{B^4}{4S^2} - \frac{B^2}{2S}\left[1 + \frac{1-2\nu}{4}\frac{2S}{B^2}\right]}}, \tag{5.4}$$

wherein l_e is the average length of the element, B the largest dimension and S the surface area of the finite element. The first root consists of the compression wave, multiplied with a factor α_t, which depends on the type of element, described by Zienkiewicz & Taylor [2000].

5.2 Validation

To verify the correctness of the PLAXIS dynamic analysis, some semi-analytical solutions are performed. Firstly the arrival time of the Rayleigh wave is checked conform the equation of motions and their respective equilibrium equations for homogeneous soil. The Rayleigh wave is depending on the primary and shear wave velocity. This relation was described by Lord Rayleigh [Pichugin, 2008]. For verification the time is normalised so that the surface displacement of the tested frequency range are occurring at the same normalised time. This is illustrated for the surface displacement at the source and at a distance of 10 metres from the source in Figure 5.3. This figure shows that the estimated arrival of the Rayleigh wave matches the start of the harmonic displacement at a distance of 10 metres from the source point, thus based on this check, the data is considered as valid.

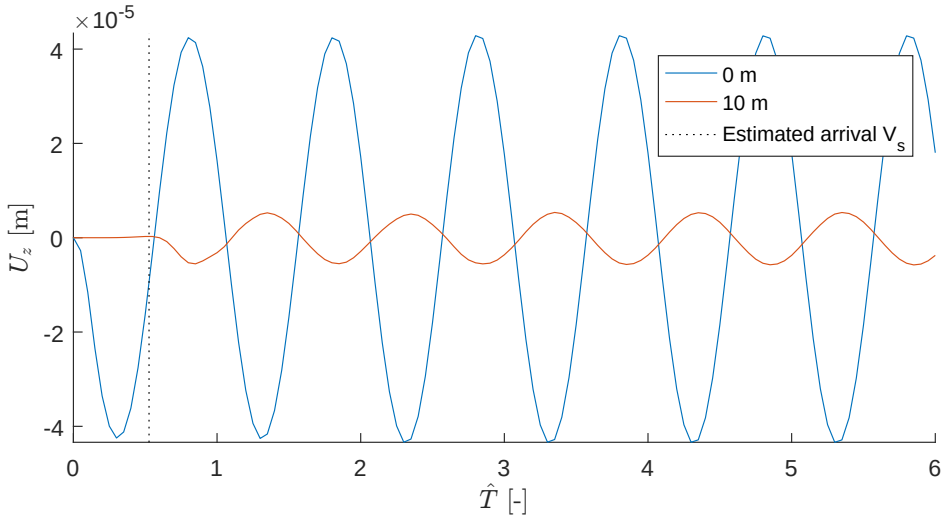

Figure 5.3: Time series of surface displacement.

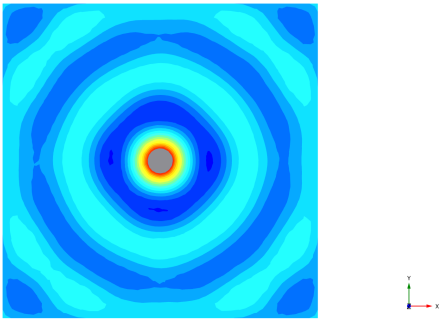

Furthermore, with wave propagation at the surface it is known that for homogeneous cases with only a slab foundation, that the displacement spread radial from the source point. From Figure 5.4 it can be seen that this is valid for this model.

Figure 5.4: Displacement distribution at 1s (8Hz).

5.3 Homogeneous soil analyses

In this part, a relation for the surface amplitude is analysed for different parameters. The objective is to harmonize the comparison and make it scalable for other cases. Firstly the slab foundation is investigated and subsequently the pile foundation is further analysed.

In the analysis, the following parameters are used:

Symbol	Description	Unit
r_s	Radius slab foundation	[m]
A_z	Amplitude	[m]
V_r	Velocity Rayleigh wave	[m/s]
p	Uniform surface load	[kN/m^2]
r	Radius from source point	[m]
f	Frequency	[Hz]
L_p	Length of pile foundation	[m]
r_p	Radius pile foundation	[m]
H_n	nth-Layer depth	[m]
K	Bulk modulus	[kN/m^2]
μ	Lamé's constant (Shear modulus)	[kN/m^2]
ν	Possion's ratio	[−]
ρ	Material density	[kg/m^3]

5.3.1 Slab foundation

In this section, the slab foundation is further analysed. To scale the model to other type of soils or properties, the results are normalised. For the displacement at the surface, the method described by Love [1929], which defines an uniform distributed load in a circular area in relation to displacements in rings, is used. This displacement is expressed as

$$u_z = \frac{2p(1-\nu)}{\pi\mu}\left[\int_0^r K\left(\frac{r}{\rho}\right)\mathrm{d}\rho + \int_r^{r_s}\frac{\rho}{r}K\left(\frac{\rho}{r}\right)\mathrm{d}\rho\right], r \leq r_s, \tag{5.5}$$

and

$$u_z = \frac{2p(1-\nu)}{\pi\mu}\left[\int_0^{r_s} K\left(\frac{r}{\rho}\right)\mathrm{d}\rho\right], r \geq r_s. \tag{5.6}$$

A combination of both equations, results in a static response due to gravity of the structure on the soil, which can be expressed as

$$A_{z,0} = \frac{pr_s(1-\nu)}{\mu}. \tag{5.7}$$

To normalise the frequency, the radius of the slab in relation to the Rayleigh wave velocity was used. The result is illustrated in Figure 5.5, which shows the amplitude of the dynamic accelerated force related to the frequency and its position for both sand and clay soil types. $A_z(f)$ is considered as the amplitude of the steady state response, this is obtained by running the whole time series and using only the last 2-3 periods of sinusoidal response. However, this steady state was not fully observed in at a certain frequencies. Although the material properties, see Table 5.1, and obtained time series differs much, the method for normalisation is sufficient. At lower frequencies $f\frac{r_s}{V_r} < 0.25$, the amplitude has reached a maxima, although it has several tips and dips. When reaching higher frequencies, the amplitude decreases significantly on exponential scale. At higher frequencies $f\frac{r_s}{V_r} > 1$, i.e. the radius of the slab is equals to the wavelength, the amplitude tends to be similar to the source amplitude. When the radius of the slab is near half of the wave length, the amplitude decreases drastically. The low amplitude at higher frequencies is due to the effect that the interface between the slab and soil does not contains one period or only a tip or dip, but multiple periods, which causes interference towards each other.

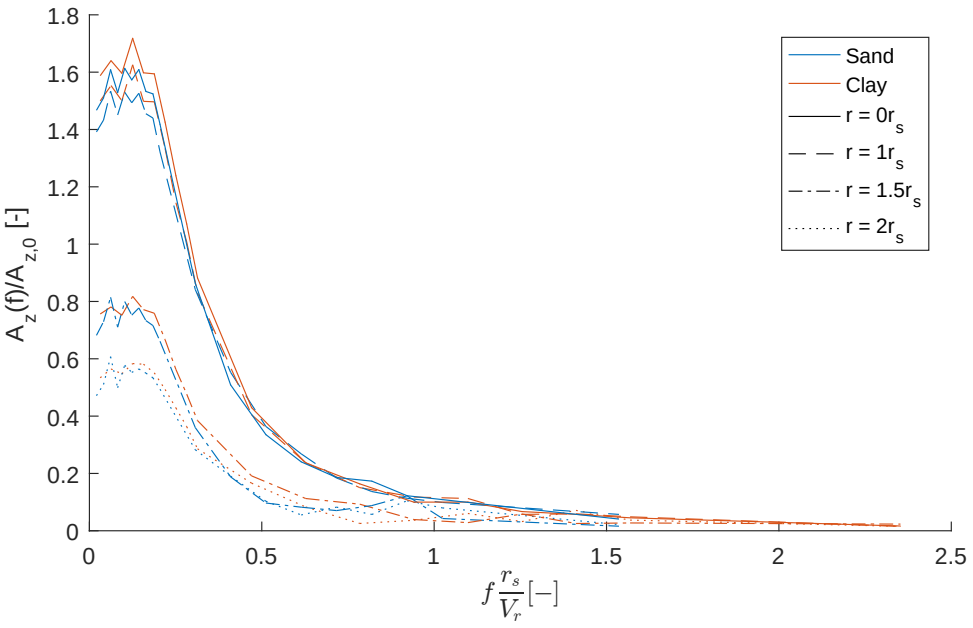

Figure 5.5: Steady state response for homogeneous soils and slab foundations.

5.3.2 Pile foundation

The dynamic interaction between soil and piles is a challenging subject for geotechnical researchers. For comparison, the same non-dimensional conversions were used compared to previous section. Figure 5.6 illustrates the influence of a pile foundation relatively to the surface amplitude. Overall, results obtained by pile foundation follows a similar distribution

of amplitudes compared to only a slab foundation. At $f\frac{r_s}{V_r} < 0.25$ a maxima was reached. For distances close to the foundation, the influence of a pile foundation is around 25%, for distances further away, the difference between a pile and no pile foundation is almost neglectable. At higher frequencies, $f\frac{r_s}{V_r} > 1$, the difference between a pile foundation and no pile foundation is limited to 10%.

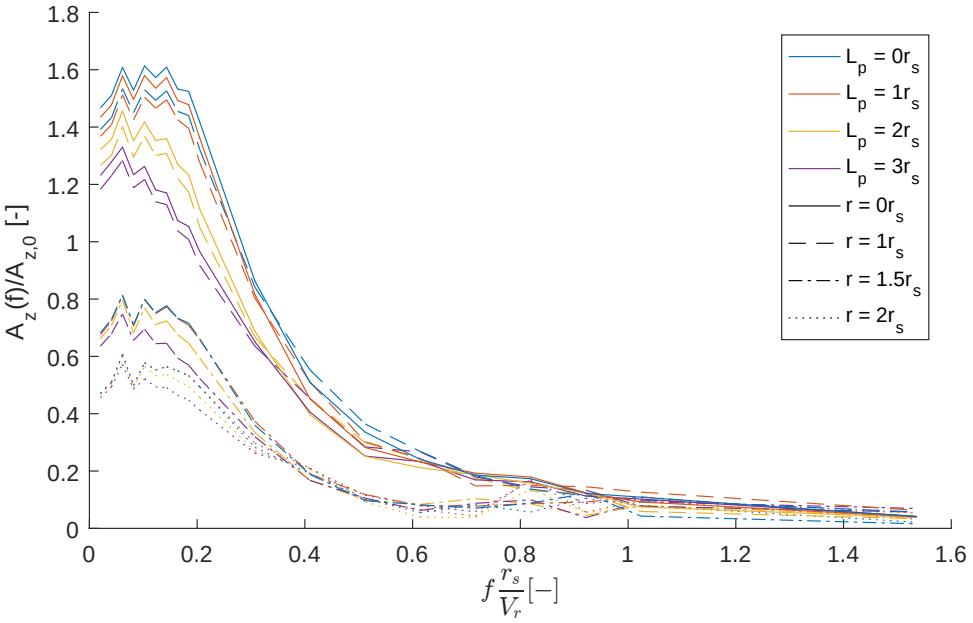

Figure 5.6: Steady state response for homogeneous soil and different pile lengths.

5.4 Layered soil analyses

In this part of the analyses, the layered soil model is introduced. It is assumed the layers would have influence on the actual amplitude obtained by receiver points. Similar as the whole model, the layers are in relation to the radius of the concrete slab foundation. The parameters used for normalisation are similar as mentioned before. However, Lamé constant μ, Poisson ratio ν and Rayleigh velocity V_r are based on the properties of the top layer. The results are limited to $2r_s$ in distance from source point and $H_1 = 4r_s$ for layer depth, to obtain an overall view of the results.

5.4.1 Slab foundation

The first model conducted consists of a slab foundation and different layer depths. A comparison with the homogeneous soil model was made, by adding this result in the graph. The obtained results from this analysis are illustrated in Figure 5.7. With referring to this figure, the overall amplitude with a layered model is greater compared to a homogeneous

model. Interestingly, where the homogeneous model (blue line) has a plateau with a few ups and downs for frequencies below $f\frac{r_s}{V_r} < 0.25$, layered models tends to have a single peak value. The frequency wherein this peak is obtained depends on the layer depth. For $\frac{H_0}{r_s} = 1$ (red line) this occurs on $0.25 \cdot f\frac{r_s}{V_r}$, $\frac{H_0}{r_s} = 2$ (yellow line) at $0.19 \cdot f\frac{r_s}{V_r}$, $\frac{H_0}{r_s} = 3$ (purple line) at $0.16 \cdot f\frac{r_s}{V_r}$ and $\frac{H_0}{r_s} = [4,6]$ (green, light blue and dark red line) at $0.10 \cdot f\frac{r_s}{V_r}$. Increasing towards higher frequencies, i.e. $f\frac{r_s}{V_r} > 0.5$, results in similar amplitudes for all tested layer depths.

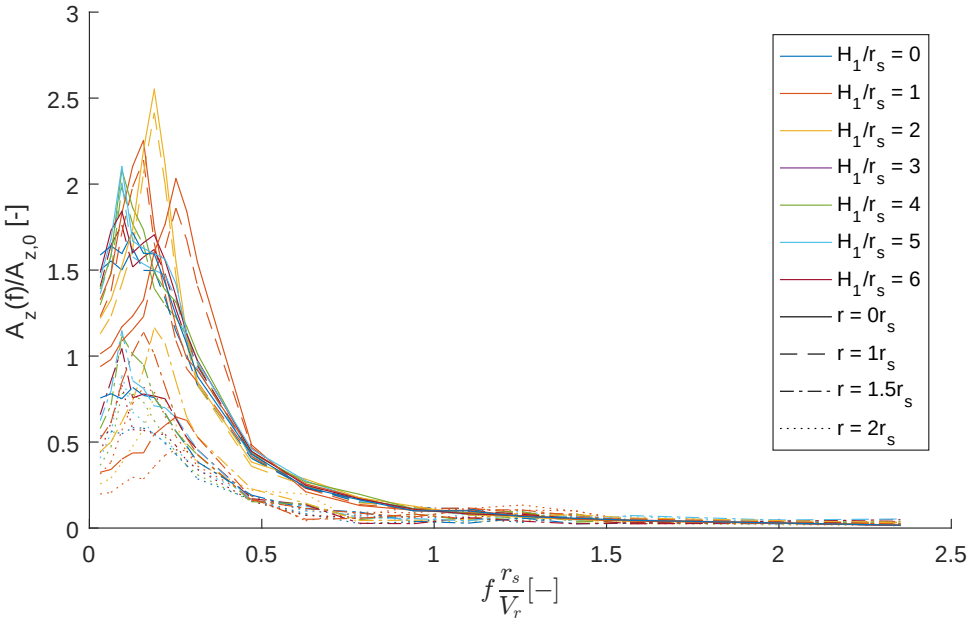

Figure 5.7: Steady state response for layered soils and slab foundations.

5.4.2 Pile foundation

Similar to piles in homogeneous soils, the piles in layered soils were tested in the same manner. In Figure 5.8 is the result illustrated. In order to make it more structured, the result is limited to $L_p = [0r_s,5r_s]$ and $H_1 = 3r_s$, in relation to a slab foundation on homogeneous soil. A higher ratio of layer depth was resulting in similar distributions for piles.

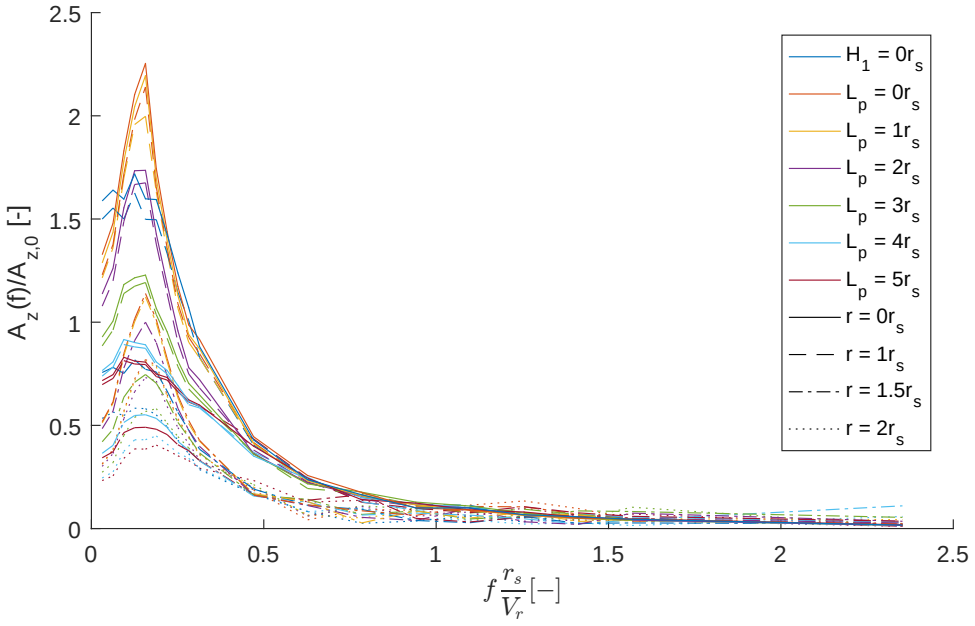

Figure 5.8: Steady state response for layered soil ($H_1 = 3r_s$) and different pile lengths.

Figure 5.8 illustrates the obtained results normalised with coefficients as mentioned before. Looking at lower frequencies, $f\frac{r_s}{V_r} < 0.5$, the amplitude of different models follows an unique path. The effect of the pile is at this point significant. At higher frequencies than this point, the pile foundation could be neglected to archive similar results. The location of the maximum amplitude does not change by introducing a pile, only the amplitude itself is lower. Interestingly, at specific positions, the obtained amplitude is slightly higher than the amplitude of the source foundation.

Based on the steady state response, amplitude differences based on distances is not clearly illustrated, thus Figure 5.9 illustrates the amplitude distribution over position for different pile lengths at $f\frac{r_s}{V_r} \approx 0.5$. The graph shows clearly visible that the pile length has a significant influence on the amplitude at a certain distance from the source point for layered soils. Interestingly, when the depth in the stiffer soil increases, the actual amplitude measured at the foundation increases again. The effect of the pile starts to be visible at some distance away from the source, thus the pile can not be neglected in layered cases.

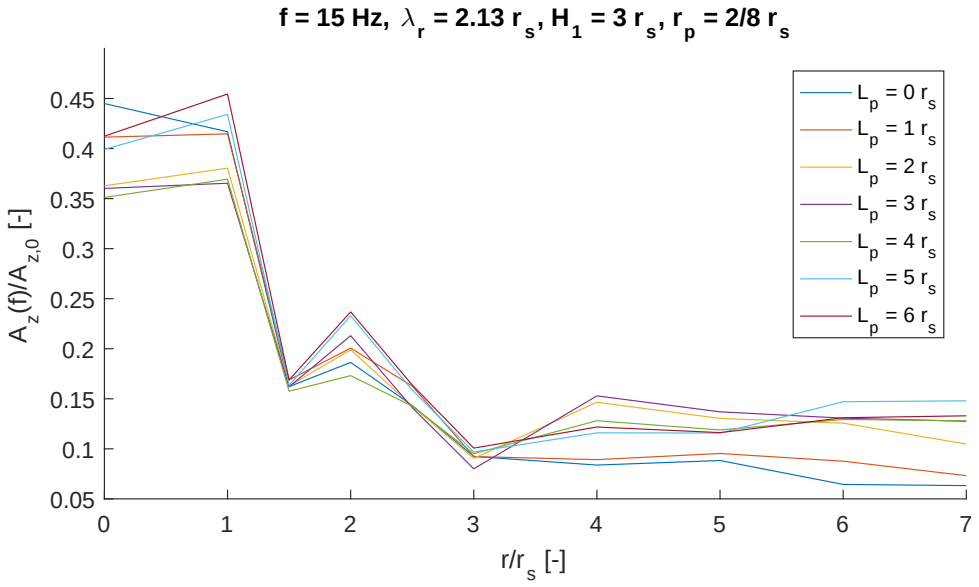

Figure 5.9: Non-dimensional amplitude at different positions.

To illustrate this behaviour better, a figure is introduced which shows the harmonic displacement for a specific frequency and position, as function of time. Figure 5.10 consists of two graphs, the first illustrates the displacement in time domain. The two vertical lines are the assumed arrival time of the Rayleigh wave from the underlying layer and the top layer. It can be said that a layered model results in an earlier starting harmonic displacement, compared to the homogeneous model. This effect is caused by a wave transmitted into the underlying soil creating a Stonely wave at the interface. Another interesting point in this graph is the time that it takes to develop a stable solution. For layered soils is this significantly longer than homogeneous soils, whereas homogeneous soils are nearly direct stable. For comparing this to Padrón et al. [2012] theory, it can be said that this is not valid when looking into the overall time series at a specific distance. The second graph in this figure illustrates the measured frequencies of the time series, when the harmonic force is applied at 20 Hz. It is assumed that the peak frequency will be at 20 Hz. For all illustrated combinations, this is valid. However, when a pile penetrates the underlying layer, this peak is not significantly. It has several small peaks in the near frequency range, which are half the magnitude.

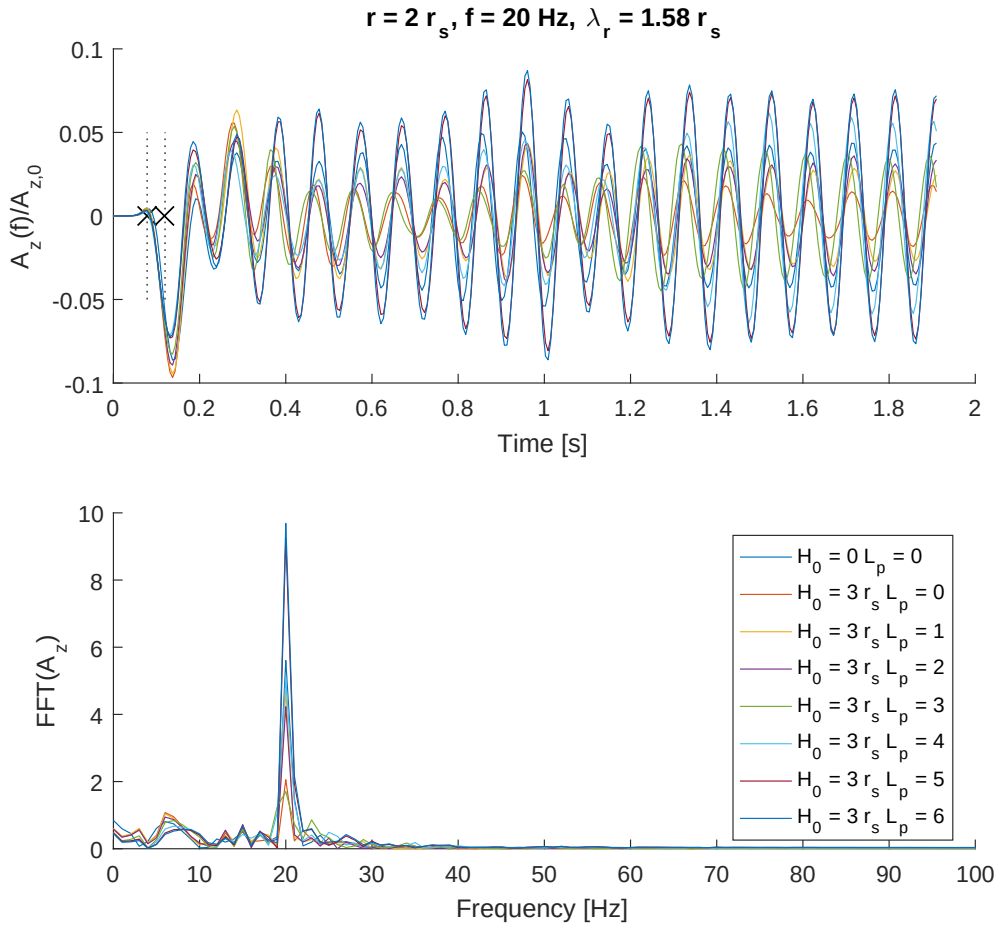

Figure 5.10: Harmonic displacement.

5.5 Slenderness of pile

As described by Deng et al. [2014], the slenderness of the pile might influence the result significantly. To obtain results of slenderness influences, the test was performed in layered soil at a specific frequency and the changing variable is the pile radius. This is changed in acceptable ranges in relation to the slab radius. This model has been calculated in time domain. To obtain the results in frequency domain, only the last half a second of the time series is used, when the harmonic displacement shows a stable behaviour. The amplitudes are illustrated in Figure 5.11. The maximum measured radius is 20% of the dominant shear wavelength, which results in a relatively error of 1.2% according to Equation 5.1.

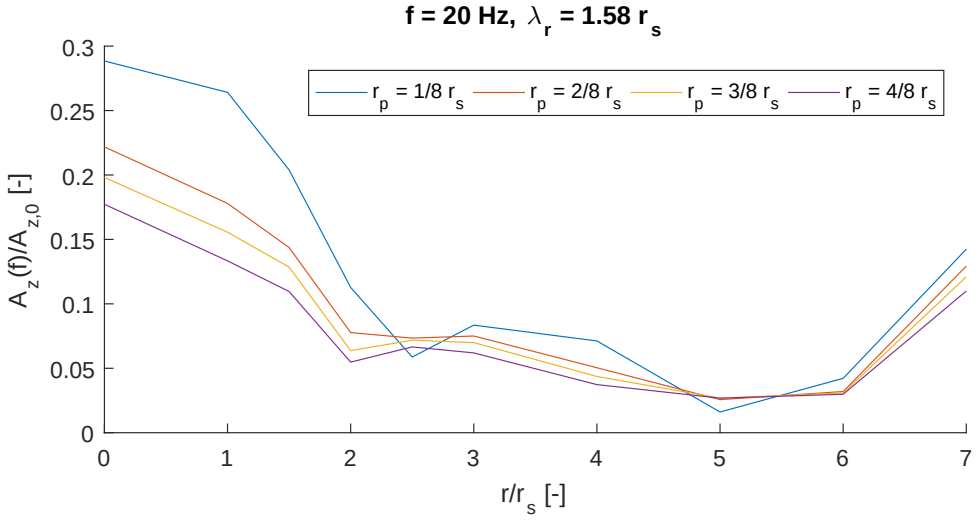

Figure 5.11: Amplitude at different positions.

When observing Figure 5.11 interesting patterns were obtained. As assumed before, a larger pile radius results in more surface in which the forces can be transferred from the pile foundation to the surrounding soil. The local stiffening effect around the pile has as result that the smallest pile diameter has the largest amplitude at the surface and vice versa. Some distance away from the source, the amplitude decreases towards a similar amplitude. Interestingly, at a distance much further away, the amplitude increases in value. This might occur due to the existence of a boundary and not all waves are getting perfectly absorbed. Thus, to verify the obtained amplitude at $7r_s$, a larger model is required to reduce the artificial boundary effects. Overall, the theory of influence on the displacement is valid, although compared to the length of the pile it is not significantly, since the pattern remains the same.

5.6 Pulse load

In previous sections a harmonic force is placed on top of a foundation. This section will introduce a pulse load on a foundation and its influence to the surrounding soil. The applied pulse load consists of a force with the same magnitude as applied during harmonic loading. By introducing a pulse load on the structure, the behaviour of the harmonic waves is reduced to one single sinusoidal period and the resulting impact on the surrounding soil can be better observed. In this particular case is it possible to determine reflection and refraction of a single wave induction.

The observed time series is illustrated in Figure 5.12. After applying one sinusoidal cycle, the response illustrates a dip. This dip is due to the effect that the motion in vertical direction results in an inertia which damps out over time. At the receiver point in the soil

some interesting effect happened, when a layer is present, the first dip in the graph is not the lowest one, similar as at the source, but the second one instead. This can be due to some waves transmitted through the bottom soil and causing a different response at the interface which is obtained at a receiver. With the existence of layers the waves are more likely to be trapped in the layer and creating additional vertical responses after some time.

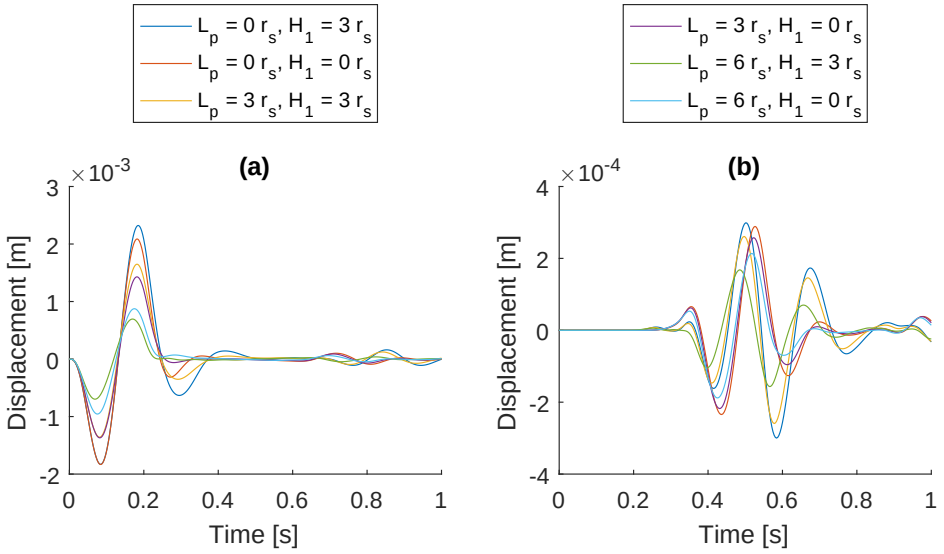

Figure 5.12: Displacement due to pulse load on source foundation (a) and at $8r_s$ receiver point (b).

5.7 Conclusion

When looking into detail in all situations, the theory proposed by Deng et al. [2014] is valid in all cases. The dimensions of the pile are critical for the amplitude at low frequencies. For the higher frequencies (above 30 Hz), the dimensions of the structure does not influence the results much. This is due to the existence of multiple wave types. Depending on the layer depth, the location and influence of a reflected wave is different. When the pile length increases and reach the interface between the layers, the arrival time at the interface away from the source point decreases significantly. The measured amplitude in the near soil increases and further away decreases. This behaviour occurs due to the pile size, since the pile radius relatively to the slab radius is small, the surrounding influence area is smaller.

For the distribution of amplitudes, the frequency of the wave and its wavelength compared to the foundation radius shows a specific behaviour. When the wavelength is larger than $2.0r_s$, the amplitudes of the harmonic displacement behaves like the theory as proposed in Section 2.3 (p. 9). If the wavelength decreases, additional waves were visible. The exception occurs when the foundation is a shallow foundation (only a concrete slab), in

this case the the additional waves (reflected and refracted) are minimal.

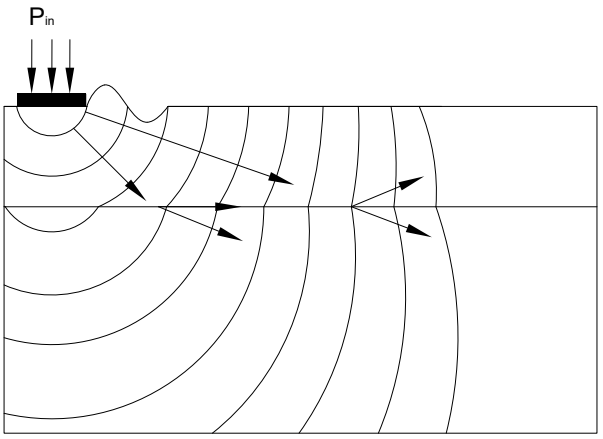

Figure 5.13: Wave propagation behaviour for slab foundation.

At low frequencies (1-10 Hz), i.e. large wave lengths, the obtained wave at the receiver behaves like a Rayleigh wave for both homogeneous soils and layered soils. For higher frequencies, the homogeneous model remains with the same pattern, a theoretical Rayleigh wave. However, the layered model shows during harmonic loading no stable result in the first received periods. A peak arrives before the Rayleigh wave arrival time, which is caused by the underlying layer and this might result in the occurrence of a Stonely wave. Depending on the location, the time required to obtain stable results increases. The response does not show only a Rayleigh wave, but also some interference at the surface. This happens due to reflection at the interface between the layers. Whereas around the artificial boundaries the waves are not fully absorbed, which causes some reflection back towards the receivers.

A suggestion based on this study is to limit the model for the required distances to obtain a stable solution in a shorter time and introduce damping. For continuing, the parameters which might influence the results of this study are layer depth, pile length and ratio between different type of soils (body wave speeds). However, the pile length might not influence the results much in homogeneous soils and could be omitted.

Chapter 6

Interaction of two foundations

Within previous chapter, the different parameters and their influence on soil response were explained. In this chapter, several foundation configurations are further studied to obtain relations in wave propagation patterns. In the first section the geometry and material properties are explained, following with analyses of the different foundation configurations and their respective propagation patterns. Finally, a suggestion for further studying the behaviour is proposed.

6.1 Geometry and Material properties

As mentioned earlier, the aim of this project is to investigate different wave propagation patterns for shallow (slab) and deep (pile) foundations. Similarly to other calculations, a three dimensional finite element model was made in PLAXIS 3D. The model consists of two structural objects, a source and receiver. The source is accelerated with a force at a certain frequency, whereas the model has a homogeneous and layered configuration. Figure 6.1 illustrates the geometry of the 3D-model in x-z plane. It is assumed that the structural elements consists of circular cross sections. Furthermore, to enhancing scalability of the model, all dimensions are relatively to the diameter of the foundation, D_f ($D_f = 2r_s$). Due to time limitations, only the layer depth $H = 3D_f$ and pile dimension $D_p = \frac{1}{4}D_f$ were analysed. Based on previous study, it is less likely that the slenderness ratio results in significantly different results. The distance d is $2^{N_t}D_f$, where N_t varies through different configurations. The length if the piles, L_1 and L_2 are also varying throughout the models.

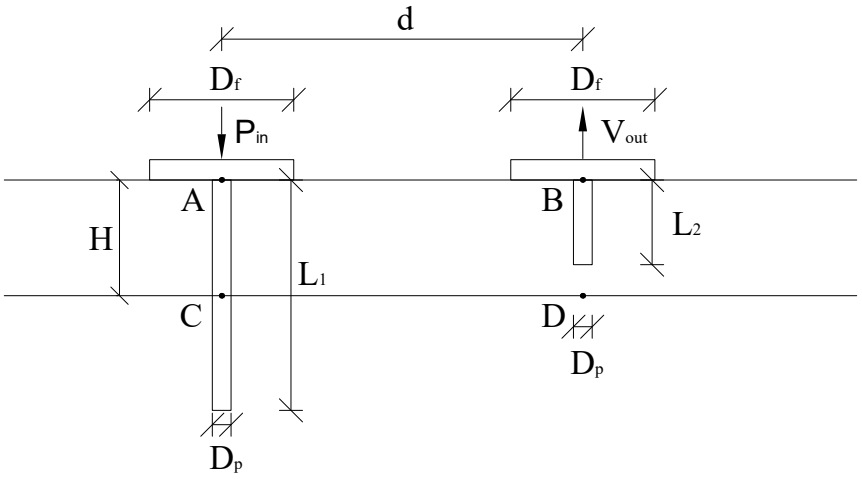

Figure 6.1: Geometry of tested model.

Both soil and foundation are assumed to behave linear-elastic. Thus, in this model the theory from Chapter 2 (p. 5) can be applied. The used material properties are described in Table 6.1. Two different soil configurations were analysed, a layered model, which consists of a soft layer over a stiff half-space, and a homogeneous model, which has only a stiff half-space. The slab foundation and the piles were modelled with the same material properties, concrete. The force P_{in} acts on the source footing as uniformly distributed surface load and has a magnitude of $10\,\mathrm{kN/m^2}$.

Table 6.1: Used material properties.

Soil Type	Unit	Soft	Stiff	Concrete
Mass density ρ	[kg/m^3]	1500	2200	2500
Young's modulus E	[MPa]	45	1500	30 000
Poisson ratio ν	[-]	0.48	0.30	0.25
P-wave speed V_p	[m/s]	508.4	1036	3759
S-wave speed V_s	[m/s]	99.71	497.7	2170

A suggestion from previous chapter, Chapter 5 (p. 35), was the use of Rayleigh damping. The damping ratio $\xi = 2\%$, was used on the first two frequencies representing the first modes of the top soil layer. Figure 6.2 illustrated the finite element model. Boundaries applied to the soil, marked BC1, BC2 and BC5 have viscous conditions, i.e. the wave gets fully absorbed, BC4 is a fully free and BC3 functions as plane of symmetry. The dimension of the model is depending on the configuration. A Rule of thumb that was used is that the horizontal dimension from the source was the maximum value of $2d$ and 0.1λ. In vertical direction, the model size is equal to the maximum of $2L$ and two times the horizontal direction.

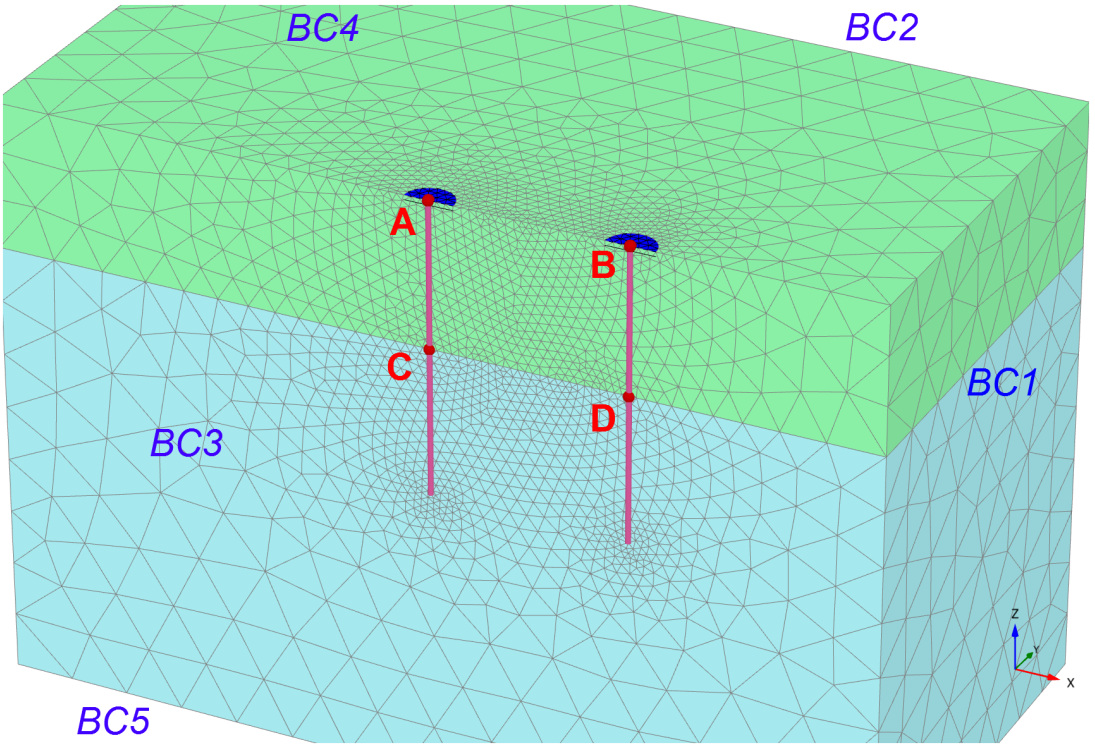

Figure 6.2: Three-dimensional finite element model of foundation and soil.

Based on previous chapter, it can be assumed that the layered model will have a more interesting time series than the homogeneous case. Thus, the following sections are focused on the time series of layered cases in a mid-range frequency. The tested cases are described in Table 6.2.

Table 6.2: Test cases.

Test name	Case nr.	L_1	L_2	f [Hz]
Slab-Slab	1	$0D_f$	$0D_f$	30
Pile-Pile	2	$6D_f$	$6D_f$	30
Slab-Pile	3	$0D_f$	$6D_f$	30
Pile-Slab	4	$6D_f$	$0D_f$	30

6.2 Slab-slab interaction

The first configuration consists of two shallow foundations (test case 1, Table 6.2 (p. 51) based on Figure 6.1 (p. 50)). The graph itself contains four different colours, which matches the different distances relatively to the diameter of the slab. The source response is dashed, where the colour of the lines matches the distance (calculated through separate models. All lines have an offset from the zero point of the graph based on the distance d from the

source and a certain factor to distinguish all lines. The black dashed-dotted line is the arrival of the P-wave of the soft layer, and almost the arrival time of the S-wave of the stiffer layer. The black dotted line is the arrival time of the S-wave.

Figure 6.3 illustrates the relation over time and by distance. The first response is scaled for visibility of the whole model. The source foundation was accelerated with a pulse load, i.e. one sinusoidal period. This period results in the first peak visible, where after the force is abruptly stopped. This force was transmitted to the stiffer soil and partly reflected back to the foundation. Looking at $d = 2D_f$, a small peak occurs before the arrive of the S-wave and Rayleigh wave of the top layer. However, the receiver foundation follows the vertical response, which results in the first small peak. The second peak, received after the S-wave arrival time was limited in actual response. This is due to the interface between the layers has a maxima slightly after the maxima of the surface layer. This effect of two waves propagating with a different wavelength happens throughout the whole model, where this effect has a certain influence on the actual height of the arrived peak amplitude at the receiver. Interestingly, at the largest distance $d = 16D_f$, the Rayleigh wave was not the most dominant wave. The wave caused by interference, i.e. trapped in the layer, causes the highest magnitude.

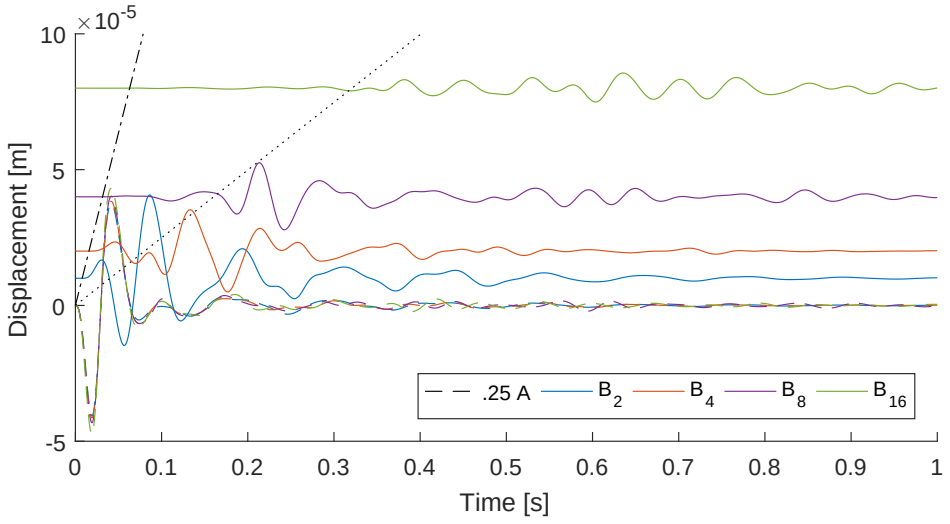

Figure 6.3: Time series of responses with shallow foundation for source and receiver (offset $5 \cdot 10^{-6}d$).

6.3 Pile-pile interaction

Another basic configuration excited with a pulse load consists of two pile foundations (test case 2, Table 6.2 (p. 51) based on Figure 6.1 (p. 50)). The parameters used were similar to previous output and similarly the figure consists of the same type of lines. Only in this case the scale of the source response is slightly lower. In the slab-slab interaction a small

wave propagating at the sub-surface layer arrived earlier than the actual Rayleigh surface wave. In this model it is expected that this effect will happen even more, due to the direct transmission from the pile foundation into the stiff layer and its receiver located partly in the stiff layer.

Figure 6.4 illustrates the obtained results from this analysis. In similarity to previous model, the first peak at $d = 0$, the coloured dashed lines, exists when the force was applied and it will take afterwards some time before this peak damps out. However, as seen mainly for the larger distances, the rate wherein it damps out is not the same for every distance d. This indicates some degree of structure-soil-structure interaction existing for pile foundations. Interestingly, similar to the slab foundation the stiffer layer and soft layer have both a wave propagating with a different speed. At $d = 2D_f$ this results in a large first wave occurring slightly before arrival time of the S-wave. However, due to this first wave, the second peak reduces in amplitude, whereas this effect was not seen at larger distances. As seen from the figure, when $d = 4D_f$, the first peak was received through the underlying layer and was slightly smaller than the actual Rayleigh wave. The response at the receiver indicates some wave interference at the receiver. As known from this receiver response, it is expected to happen also at $d = 8D_f$ and $d = 16D_f$ in a similar way. At $d = 16D_f$ there were even two significant peaks with a higher magnitude received before arrival of the Rayleigh wave. Another interesting effect is that when the distance d increases, the time before this single wave damps out increases significantly.

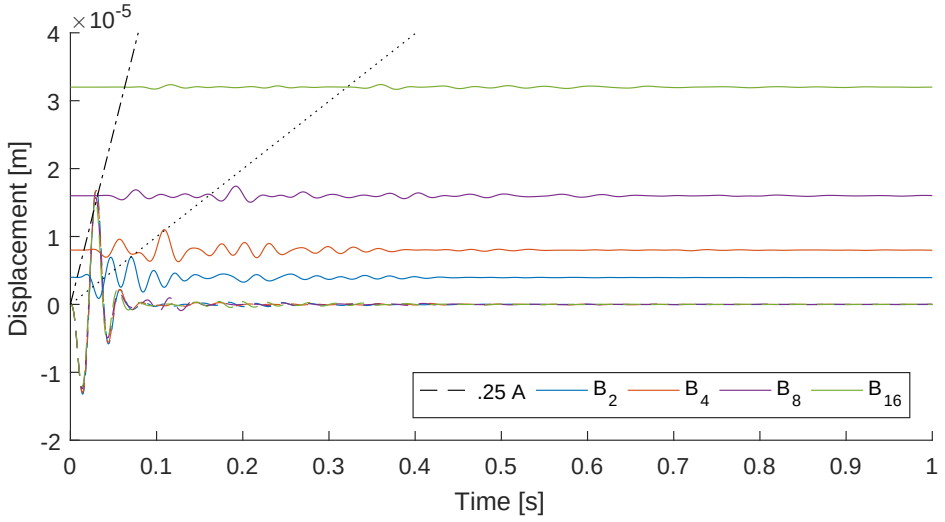

Figure 6.4: Time series of responses with deep foundation for source and receiver (offset $2 \cdot 10^{-6}d$).

6.4 Slab-pile interaction

Based on the previous types of foundations a combination between these foundations was made. In this section the results are explained wherein the source was considered as slab foundation and the receiver as pile foundation (test case 3, Table 6.2 (p. 51) based on Figure 6.1 (p. 50)). It is expected that the wave propagates with some similarity to both models.

Figure 6.5 illustrates the the vertical responses as function of time. Comparing this to previous models concludes some expectations. The response of the source was similar to the slab-slab source response. However, the receiver has no relation to any of the previous models. Only at when the receiver was positioned at $d = 2D_f$, a wave is obtained with a similar magnitude as the slab-slab interaction. When increasing this distance, this first wave still exists, only the obtained magnitude of the peak has a value which is similar to the results obtain far after the Rayleigh wave propagates and starts to damps out. After the S-wave has reached the receiver the Rayleigh wave produces a peak amplitude at the receiver. Intriguingly, the interference patterns similarly to other models as described before were reduced in this case.

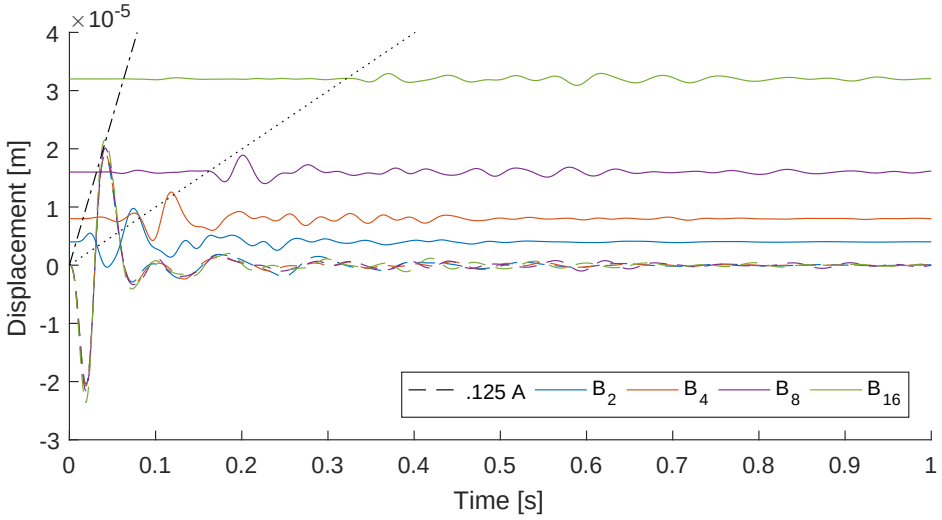

Figure 6.5: Time series of responses with shallow foundation for source and deep for receiver (offset $2 \cdot 10^{-6}d$).

6.5 Pile-slab interaction

This section describes the last, missing combination, the source modelled as pile foundation and the receiver as slab foundation (test case 4, Table 6.2 (p. 51) based on Figure 6.1 (p. 50)). Similar to all earlier situations, it is expected to have two separate peaks visible. The first peak might be better visible than the slab-pile case, due to the source which transfer

the wave directly to the sub-surface. However, the slab foundation is not able to receive this peak similar to the pile-pile interaction (through underlying soil and at the pile tip). It can be assumed that the first occurring wave is an interface wave, where the top soil follows the amplitude of the underlying layer at the interface.

Figure 6.6 contains the vertical responses for this case. The response at the source has a similar start compared to the pile-pile interaction. Only the receiver changed compared to this model. The observed response at the receiver has some similarities with the slab-slab model. However, the first wave occurring before the Rayleigh wave arrival was smaller compared to that model. At $d = 2D_f$, the wave propagation in the bottom soil creates quite some interference at the receiver. Interestingly, the interference produced reduces the actual peak amplitude and similarly the waves looks like damps out quite early, which might be a result of this effect. The effect of interference is distance independent, compared to $d = 4D_f$, $d = 8D_f$ and $d = 16D_f$. Similar to the slab-slab interaction, the vertical response at the receiver at position $d = 16D_f$ peaks due to interference afterwards.

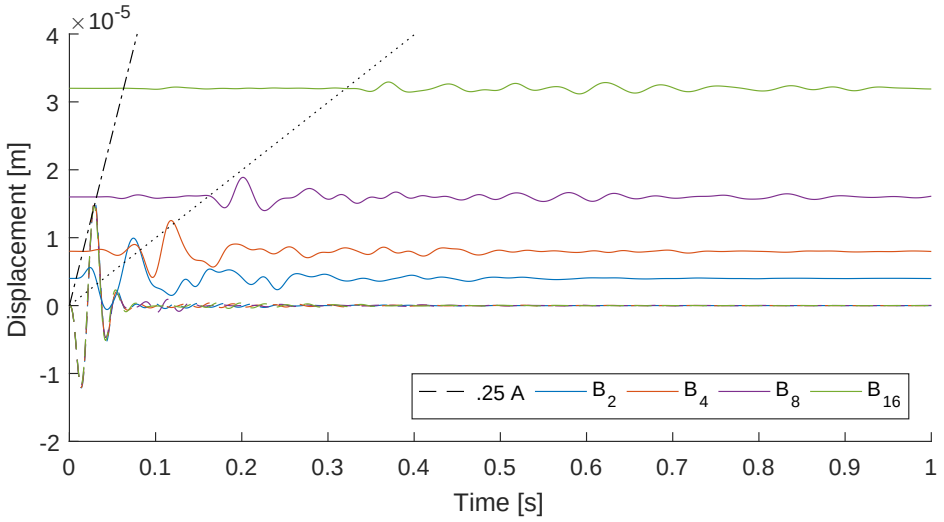

Figure 6.6: Time series of responses with deep foundation for source and shallow for receiver (offset $2 \cdot 10^{-6} d$).

6.6 Conclusion

Based on previous sections, the layered cases provides interesting results. In overall, the pattern for applied pulse loads illustrates for all cases similar behaviour if $d \leq 8D_f$, the response at the receiver point obtains two peaks with a higher magnitude, one arriving before the S-wave, which was caused by the wave propagating through the underlying soil and one surface wave afterwards which is the Rayleigh wave. However, at $d = 16D_f$, the wave with the highest magnitude was caused by interference at the receiver due to waves

trapped in the soil layer.

In Section 5.7 (p. 47) the unknown parameter for the model in harmonic configurations was the time to obtain stable solutions. Models described in this chapter which were excited with a pulse load can be used to predict required minimum time of model run for harmonic solutions. A suggested format to determine the required runtime is

$$t_{min} = \frac{N_r}{f} + C_d \frac{d}{V_s} + \frac{N_c}{f}, \tag{6.1}$$

wherein N_r is a number of sinusoidal cycles wherein the sine function will be ramped from zero to a full magnitude, C_d is a constant, which depends on the relation between the Rayleigh wave and S-wave, N_c is the number of addition cycles necessary to provide a stable solution. The numbers for this equation depends on several factors, size of the model, the presence of layers and type of foundations.

For further investigation, some limitation of model configurations is required. In this particular case, difference between source and receiver foundations would not introduce completely new patterns compared to an equal foundation, i.e. the foundation with and without piles covers most of the patterns.

Chapter 7

Vertical responses at foundations

Based on the model proposed in Chapter 6 (p. 49), a time domain analysis was performed for several frequencies and structure configurations. This analysis is time consuming, thus the number of models which are able to run were limited. The average running time for pulse loads was 16 hours each model, for the harmonic case, Table 7.1 explains the exact values in hours. The responses of the different structure configurations are explained in following sections, to conclude a comparison between the methods is made.

Table 7.1: Obtained test results and their respective calculation time for 1-50 Hz frequency range for Homogeneous and Layered soils (Harmonic loads) and system configuration.

	$d = 2D_f$		$d = 4D_f$		$d = 8D_f$		$d = 16D_f$	
	H	L	H	L	H	L	H	L
$L = 0D_f$	56:52[2]	48:19[1]	80:05[3]	53:50[3]	18:18[1]	60:02[2]	21:46[1]	44:25[1]
$L = 2D_f$	26:15[3]	45:14[3]	32:43[3]	60:27[2]	12:30[1]	36:26[4]	23:10[1]	45:01[1]
$L = 4D_f$	27:45[3]	59:43[2]	24:14[1]	47:32[3]	13:18[1]	40:58[4]	24:12[1]	49:26[1]
$L = 6D_f$	24:03[1]	31:17[1]	23:57[1]	48:41[3]	22:05[3]	72:41[3]	25:32[1]	48:39[1]

[1] Windows 10, 4 core (4.3 GHz), 8 Gb RAM
[2] Windows 10, 2 core (2.4 GHz), 2 Gb RAM
[3] Windows Server 2008R2, 4 core (2.6 GHz), 4 Gb RAM
[4] Windows 7, 12 core (2.6 GHz), 32 Gb RAM

For normalisation and make it possible to compare it with other soil types, the following factors were used in the axes

$$\begin{aligned} \phi &= f\frac{D_f}{V_s}, \\ \alpha &= \frac{A_{st}}{p\left(0.25\pi D_f^2\right)}. \end{aligned} \tag{7.1}$$

7.1 Transient response of pulse loads

The first analyses performed was a transient response analyses due to pulse loads representative for e.g. pile driving. The pulse loads consists of different periods in range equivalent for man-made environmental vibrations. Since only one single period of sinusoidal load is applied, it is assumed to result in one single peak output. However, as explained in Chapter

6 (p. 49), for layered soils, this might not be the case. The result will output the maximum obtained peak response. Although, this is not necessarily the first dominant peak in the time series, especially for layered soils. The response of pulse loads has as advantage that actual propagation patterns can be inspected with less interference. In the first part of this section, the homogeneous soil will be investigated and afterwards the layered model, with reference towards the homogeneous soil.

7.1.1 Homogeneous soil

Figure 7.1 illustrates the results of the homogeneous soil model. In overall, the results are as expected before. The Rayleigh wave is the dominant wave and diminishes over distance, with the known dissipation factor. The pile foundation itself results in marginal changes of the amplitude. At source point A a reduction of 30% was obtained, whereas at point C, the amplitude increases upto 15%. At the receiver only a 4% decrease is measured in point B and at point D this is 6%. The influence of the piles itself is limited to the response at the receiver. For this situation, a model only containing a surface footing would provide a fair estimation.

Disregarded the first dip at point B, the result at the surface is close to being frequency independent. However, the responses at point C, located at depth of H under the source and receiver, changes by frequency. The maximum value at point C is obtained at $L = 4D_f$. At this point, the pile reaches point C and transfers the loads more down to this depth. However, if a pile becomes longer, the vertical response decreases due to further local stiffening. Similar to point C, point D is frequency dependent. In addition, this frequency dependency is related to the distance. Reaching the higher tested frequencies, the vertical response decreases at point C and D with a similar rate in the figure. An exception occurs when the pile does not reach these points.

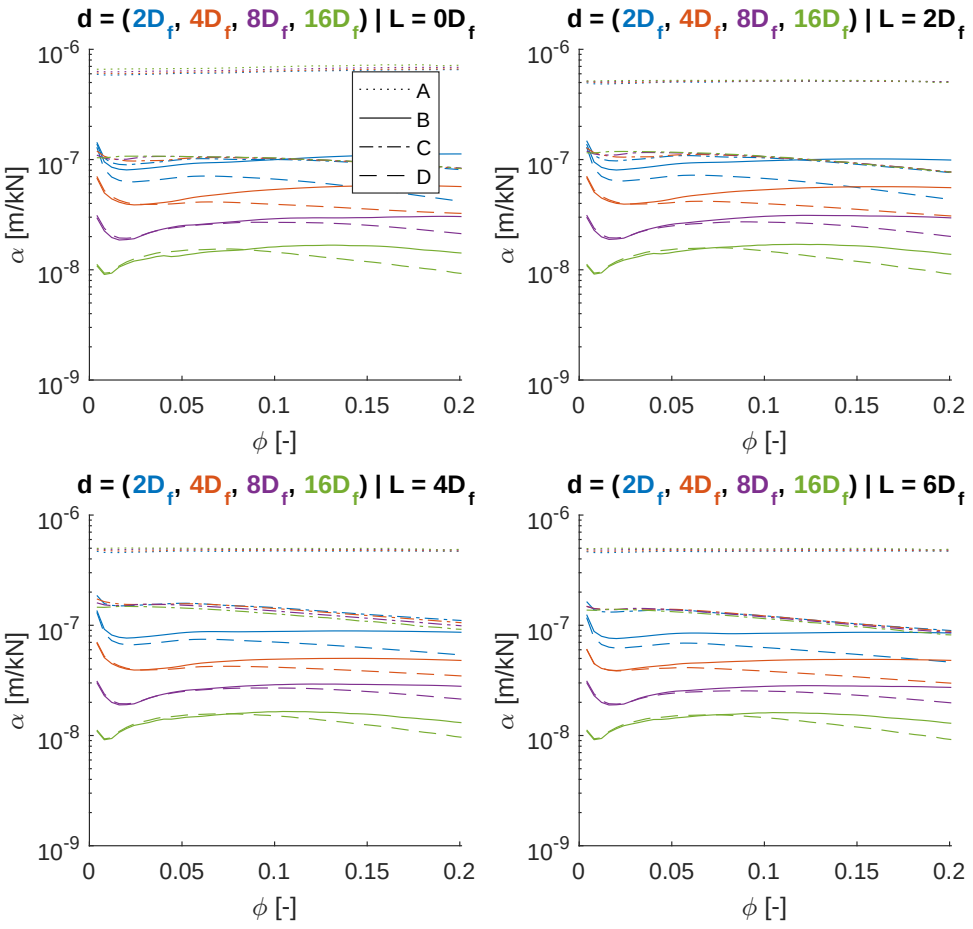

Figure 7.1: Maximum transient response at selected observation points for homogeneous soil.

7.1.2 Layered soil

When comparing the homogeneous model to the layered model, it was seen that the layered model has a stronger frequency dependency. Illustrated in Figure 7.2, without pile and with $L = 2D_f$, an overall maximum is reached around $\phi = 0.16$. However, for a distance of $d = 4D_f$, this point is reached at a higher frequency and for $d = 16D_f$ this is reached slightly earlier. From previous observations at $L < H$ it was seen that the Rayleigh wave is not the most dominant one, but the interference, i.e. trapped waves afterwords were. In all these cases, the amplitude decreases exponentially by increased frequency towards a similar level as the lowest frequencies. When the pile length reaches the half-space, i.e. $l = 4D_f$ or $l = 6D_f$, the actual peak shifts towards a higher frequency, respectively $\phi = 0.6$ for the points A and C and $\phi = 0.5$ for B and D. However, the distance $d = 2D_f$ obtains several peak values and a dip occurring in the mid-frequency range. As obtained from

earlier examination of results, the waves propagating in the top layer and the underlying layer are reducing each other at the receiver, since the wave length is not equal to each other and the wave propagation in both layers might be in opposite phase.

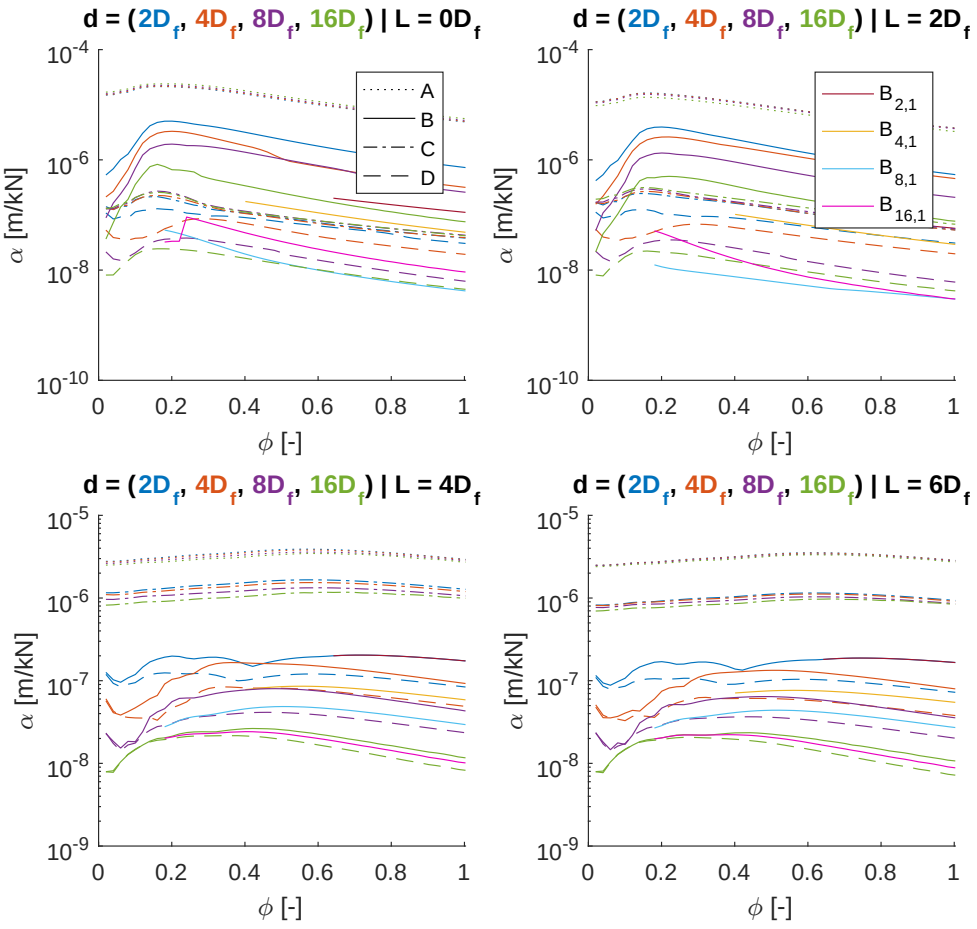

Figure 7.2: Maximum and first transient response at selected observation points for layered soil.

With referring to Chapter 6 (p. 49), the time series of layered cases have an interesting pattern, which is not clearly visible in graphs containing the maximum values. Thus, Figure 7.2 contains four extra lines which illustrates the first arrival peak before the arrival of the S-wave. This phenomenon occurs at all frequencies and distances. However at lower frequencies and shorter distances, this phenomenon can not be distinguished. A limitation is for $d = 16D_f$, where two peaks with a higher magnitude arrived before the S-wave. The relation of different distances between the source and receiver results in an interesting observation. At $d = 2D_f$ and $d = 4D_f$, the first major wave received at point B is equal to or higher than the wave received in point D. For point $d = 8D_f$ and $d = 16D_f$, the obtained peak is lower when the pile does not reach the interface. Interestingly, the obtained first

vertical response at $d = 16D_f$ is larger than the first response obtained from $d = 8D_f$. The exception occurs at $\phi < 0.23$, where the amplitude shifts strong in response from a lower value than $d = 8D_f$ towards a higher one. In overall, when the pile reaches the interface between the layers, the magnitude of the first wave is equal or higher than that in point D. For $d = 2D_f$ the amplitude is the highest peak measured at point B.

7.2 Steady state response of harmonic loading

In addition to a pulse load, the structure was exited with a harmonic load. The results used are determined by a reverse down-cross method. The assumption is made that after a specific time, obtained from the analysis with pulse loads, the harmonic excitation has reached a steady state. Thus, the last period is used as reference and backwards over the measured amplitudes, all amplitudes within a 0.1% error margin from the reference were used for this analyses. Similar to pulse loads, first the homogeneous model will be explained and consequently the layered model.

7.2.1 Homogeneous soil

Figure 7.3 illustrates the result of the homogeneous soil harmonic loads acceleration. Looking at the results, similar to the pulse load, point A and B at the surface are nearly frequency independent. Similar to pulse loads, point C and D are frequency depended. Where point C increases till the pile foundation reaches this point and then further reduces. The dependency on the frequency of point D is dependent on the distance. At shorter distances is tends to be frequency dependent on lower frequencies. At point B and D, the amplitude decays exponentially with the distance between the receiver and the source. This reduction is due to dissipation of the Rayleigh wave and similar for all frequencies.

In overall, the response at the measure points has a similar pattern compared to the pulse load. Only, the response of point C and D illustrates several tips and dips, depending on the distance. Where $d = 2D_f$ has only 3 peaks a higher magnitude, $d = 8D_f$ has 6 of them. The length of the pile has limited impact on this effect. The arise of positive and negative interference between incoming and scatterer Rayleigh waves might explain this behaviour. At $d = 16D_f$, the occurring dip at mid-frequency range is significant and afterwards the obtained steady state response at the receiver B is greater than at $d = 8D_f$ for $L \leq 4D_f$. Whereas afterwards the pattern remained the same.

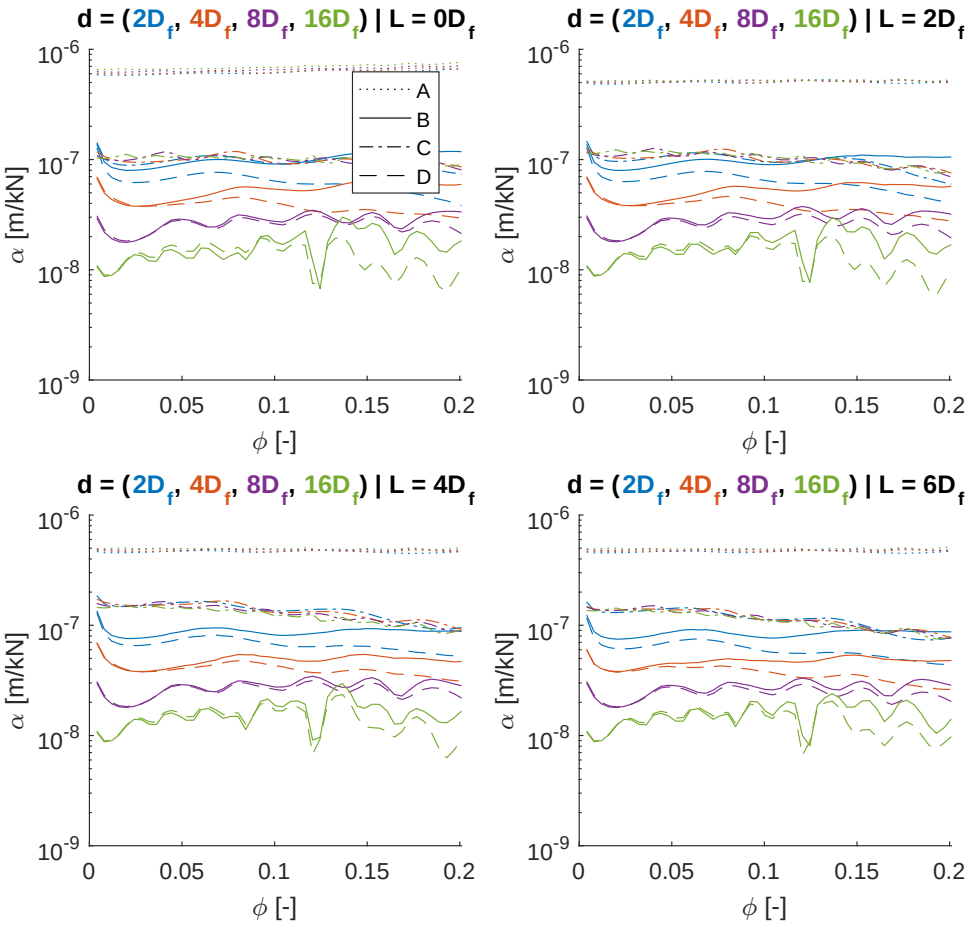

Figure 7.3: Steady state response at selected observation points for homogeneous soil.

7.2.2 Layered soil

In contrast to homogeneous soil, layered soil is more frequency dependent and has several similarities with pulse loading. Figure 7.4 illustrates the obtained results. When a pile does not reach the interface between the layers, a maximum is reached around $\phi = 0.16$. For longer piles, the frequency increases quite much towards $d = 0.7$ when a maximum magnitude is obtained. For longer piles, the frequency dependence is smaller. Point A, the source, is nearly the same for $d = 2D_f$ and $d = 4D_f$. However, at $d = 8D_f$ and $d = 16D_f$ differences are visible, thus this indicates a strong degree of structure-soil-structure interaction. Point C illustrates a similar behaviour when the pile reaches the interface.

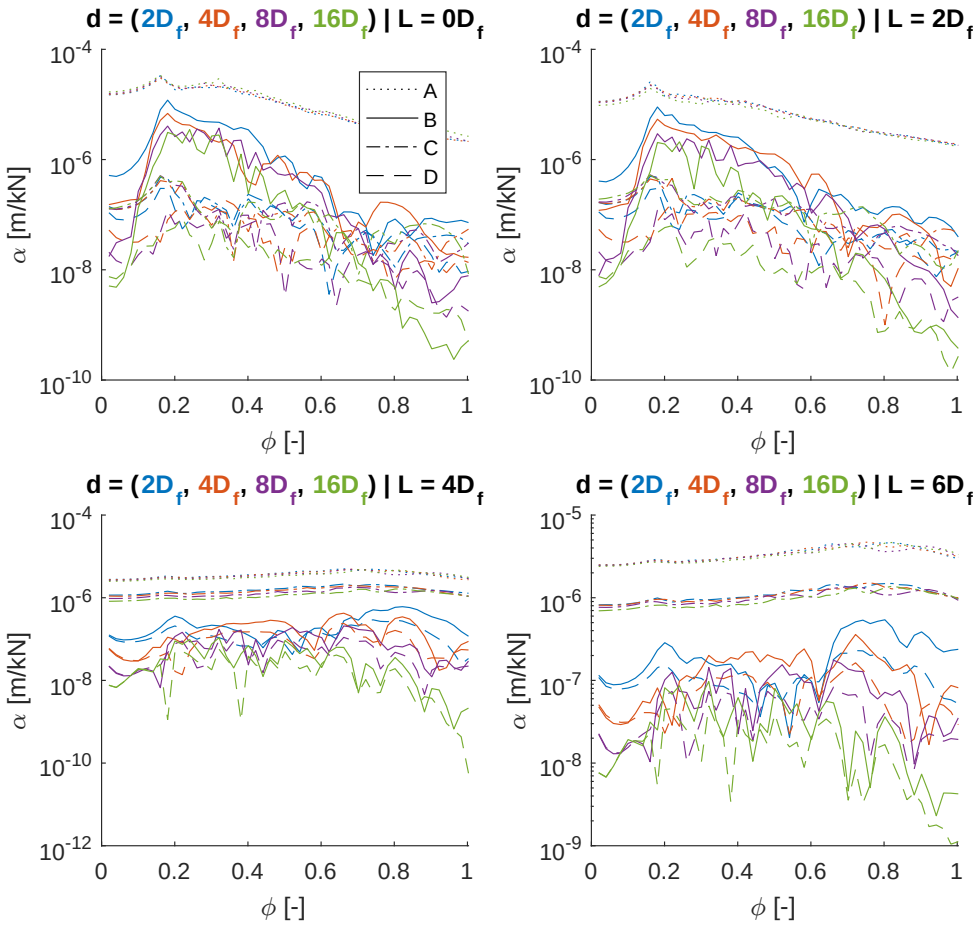

Figure 7.4: Steady state response at selected observation points for layered soil.

Point B has in this case the most interesting behaviour throughout the models. When the pile does not reach the stiffer layer, the amplitude peaks at $\phi = 0.18$ and decreases exponentially towards the amplitude at the lowest frequencies. When the pile goes into the underlying half-space, a more constant level of amplitudes is observed. However for $d = 16D_f$ the amplitude remains stable when $\phi \leq 0.8$, afterwards its decrease is more significantly visible compared to the smaller distances from the source. Compared to pulse loads, influences of waves being trapped in the top layer and creating constructive or destructive interference is overly visible by all the local tips and dips. In specific cases, mainly when $L < H$, the amplitude at interface point D reaches a higher vertical response than the amplitude at the receiver.

7.3 Comparison

Within this section, methods are proposed and verified to be able to simplify this problem. Since as is this analysis is computational intensive. Firstly, a relation of pulse loads versus harmonic loads is checked, consequently the effect of piles is better observed. Both comparisons are made for both homogeneous and layered soils.

7.3.1 Harmonic and Pulse loads

The first analysis made for harmonic and pulse loads is finding a relation how they match each other in terms of measured amplitude. In this report, the calculation has been done in time domain. Since the calculation of the pulse load is less CPU intensive in time domain, a simplification to transform harmonic loads towards equivalent pulse loads would reduce the calculation time significantly.

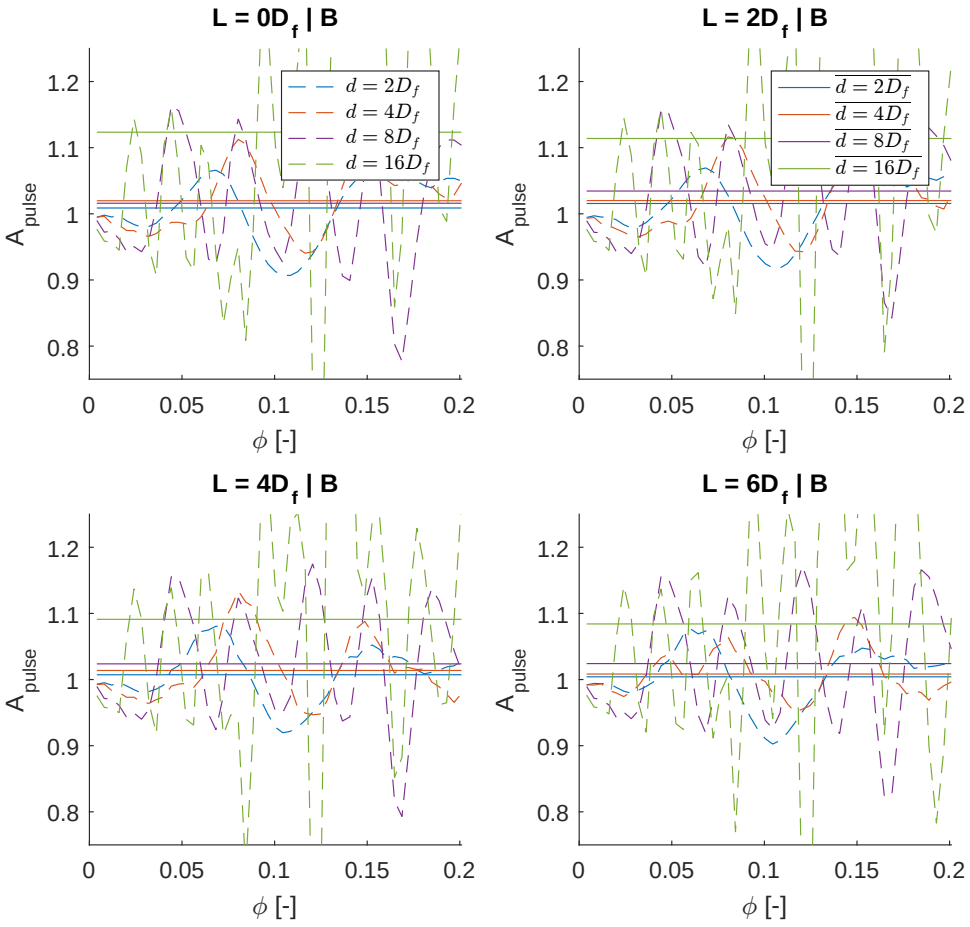

Figure 7.5: Harmonic loading relative to pulse load at receiver B for homogeneous soil.

Figure 7.5 illustrates the homogeneous soil case. Overall, the error between the models is relatively small, less than 3% when $d \leq 8D_f$. However, specific effect for harmonic loading, i.e. structure-soil-structure interaction or a possible obstructive or destructive scattered waves are not obtained during the pulse load analysis. This is visible with the single points, ranging from -25% towards +40% in worst case. Interestingly, at $d = 8D_f$ the average error compared to the pulse load is likewise, whereas at $d = 16D_f$ it decreases.

In contrast to homogeneous soil, the layered soil harmonic load versus pulse load, as illustrated in Figure 7.6, shows quite some variation. In the lower frequency range and the higher ones (when no pile exists), the amplitude of the harmonic load is likely to have an amplitude lower than the pulse load. In the situations that the pile reaches the interface, the spread of amplitudes changes almost by frequency. In overall, the average error of results between all amplitudes is 55%, whereas the total bandwidth of errors ranges from -97% till almost 300% relatively to the pulse load amplitude.

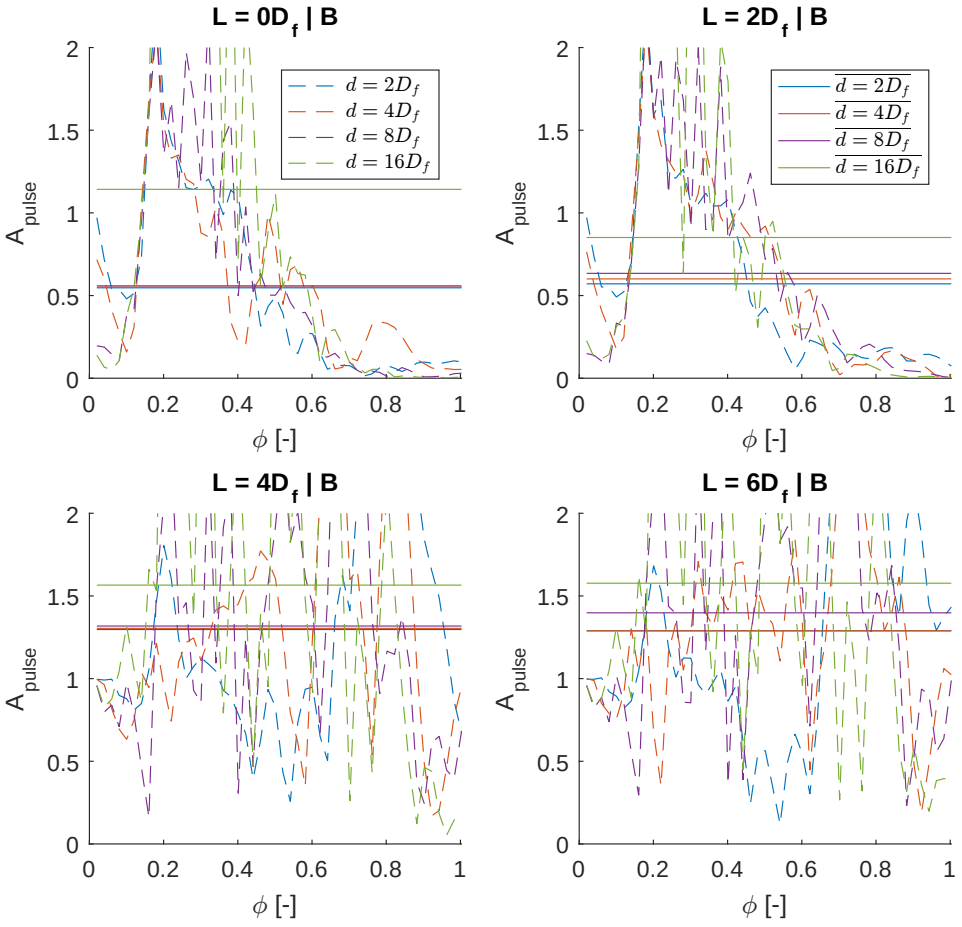

Figure 7.6: Harmonic loading relative to pulse load at receiver B for layered soil.

7.3.2 Pile length

Another simplification to the model might be related to the length of the pile. In this comparison the amplitude for a specific pile length is put relatively to the amplitude without pile foundation. In this method, the required amount of calculations can reduce significantly. The graphs are similar to all other graphs normalised based on frequency and amplitude. However, the amplitude is made relatively towards the amplitude measured at a situation without piles. The graphs are distinguished by distance.

With referring to Figure 7.7, an interesting pattern can be obtained based on distance and frequency. Especially at lower frequencies, the influence of a pile foundation on the results itself is limited. The dependence decreases by distance. Where the total bandwidth of results is 75% till 101% $A_{L=0D_f}$ for $d = 2D_f$, the total bandwidth at $d = 8D_f$ is reduced till 85% till 110%. After this distance, i.e. increasing the distance towards $d = 16D_f$, the bandwidth increases to 70% till 130%. An overall average illustrates the decrease of 15% range till 5% error at larger distances.

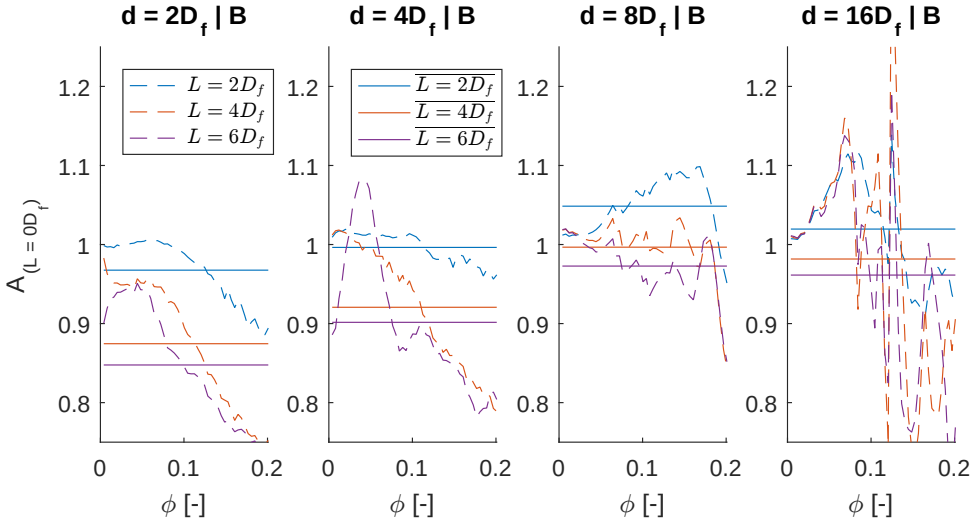

Figure 7.7: Harmonic loading relative to pile length at receiver B for homogeneous soil.

For layered soils, a similar comparison is made. Figure 7.8 illustrates the relation of the amplitude obtained with a pile compared to the amplitude obtained by only a slab foundation. In contrast to homogeneous soils, a different pattern is obtained. Where the error reduces by distance for homogeneous soils, the similar reduction is not obtained in this situation. Although, the average error decreases to a minimum at $d = 4D_f$, where after it for larger distances increases. Only at $L = 2D_f$ an average reduction is measured at $d = 16D_f$. The bandwidth of the results is compared to homogeneous soils quite high (over a 1000%). For layered soils, the higher frequencies results in a larger amplitude compared to only a shallow foundation.

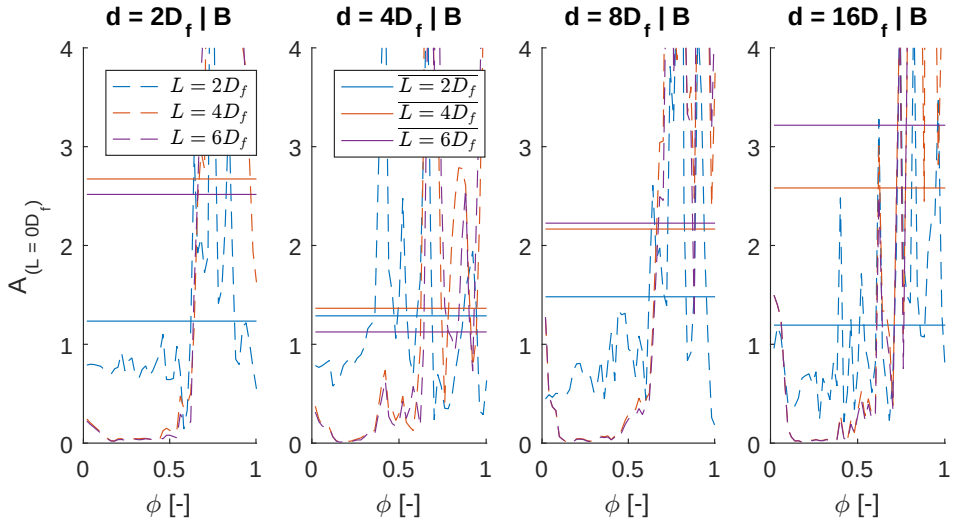

Figure 7.8: Harmonic loading relative to pile length at receiver B for layered soil.

Chapter 8

Conclusion

This report consists of a dynamic analysis of the interaction between foundations and soil. Different patterns have been obtained by performing a three-dimensional finite element analysis. The analysis consists of three different parts. A verification with known theories to decide a feasible method which has stable, reliable and consistent results. Consequently a parameter study, to obtain which parameters could influence the result and finally, a more detailed analysis of the interaction between two different foundations.

Different models proposed as analytical or finite element model are suitable for wave propagation in soils. However, both models have their own advantage and disadvantage. The analytical model only uses of surface waves. Thus, for basic Rayleigh wave propagation from slab foundations, this method could be used. Although, when modelling a second structure scattered waves are not included, and introducing a layered model, this type of analytical model disregards possible reflection and the effect of trapped waves in a soil layer. A finite element model is more feasible in these soil dynamics calculation. A two-dimensional model is a simple model, which provides reasonable results at a certain distance, includes reflection and refraction of waves. However, this model assumes, when it comes to foundations, an infinite row of foundation structures. Thus the effect of geometrical dissipation is not representative for single point loads. A more refined model, which includes a third dimension, i.e. a three-dimensional finite element model, can simulate the behaviour of geometrical dissipation from a point load. Overall, a model required to analyse this problem would be a three-dimensional finite element model. PLAXIS 3D is a commercial finite element solver which was used for this purpose.

With the use of a three-dimensional finite element model. The first situation modelled is the influence of soil stratification and structure geometry on the soil response. Several combinations were examined to obtain the influences of parameters in relation to the vertical response. All models were made relatively to the radius of the slab foundation. The pile foundation and layer depth ranges in factor to the actual radius of the slab foundation. At lower frequencies, the obtained results have a maximum, whereas at higher frequencies the measured amplitude decreases significantly. However, for layered models at higher frequencies, the existence of reflected waves, i.e. trapped waves, in the soil layer increases, similarly to the calculation time to obtain stable results. This effect changes due to the location, layer depth and wavelength. If a pile penetrates the interface towards an underly-

ing stiffer layer, the actual arrival time of a wave decreases. A first wave is measured before arrival time of the Rayleigh wave. This indicates a Stonely wave occurs at the interface and the top soil is following the vertical response of the underlying layer. The slenderness of the pile foundation has limited effect on the vertical response. Overall, the parameter considered to have influences on the results are layer depth, pile length, receiver distance and relation of soil properties between the layers.

Finally, two foundations, shallow and deep foundations, were analysed for different soil stratifications by a similar three-dimensional finite element model. A homogeneous half-space was used as reference to a layered ground consisting of a soft top soil with an underlying stiffer half-space. The analysis was made for a pulse load and harmonic loading. A pulse load was examined in time domain for propagation patterns and used to determine stable times for a harmonic excitation. The pulse loads tend to have at least two peaks with a higher magnitude in layered cases. This effect is similar as described above. The wave in the underlying layer propagates faster than in the top layer. For larger distances, in some cases it was observed that neither the Rayleigh nor Stonely wave caused the peak response, but instead the interference due to trapped waves afterwards. The harmonic excitation results were proposed in frequency domain. The steady state response to harmonic excitation of homogeneous soils was found less frequency-dependent compared to layered soils. In both cases, some degree of structure-soil-structure interaction was observed. In the layered model, the response at the receiver foundation showed a strong dependency of frequency, due to trapped waves in the soft layer, forming interference. In overall, the response between the pulse loads and harmonic loading tends to be following a similar trend. However, for both soil models this might be the case, disregarded oscillation observed at the receiver. The complex interference patterns could not develop in pulse loads, where they exists during harmonic loading. It tends that the homogeneous model has less influence of that behaviour compared to the layered model. Introducing piles, have led to a difference of 2% till 15 % for homogeneous soils, with the larger distances as less influences. In contrast to layered soils, were the differences is at least 40%. Interestingly, similar relation with distances as homogeneous soils was not found.

To conclude, wave propagation in soils is fairly hard to estimate. It relies on several factors, such as structure dimensions and soil stratification. In both tested situations an estimation can be obtained by performing a pulse load. However, local side effects due to interference is disregarded. A more suitable change is omit a pile foundation. This could be done for homogeneous soils, where it tends to have a limited influence and for distances further away, the influence is neglectable. For layered cases it is important to model the pile foundation correctly, due to much interference what partly happens because of the existence of the pile foundation.

Chapter 9

Reflection

With this chapter, the results will be evaluated with other methods from theories and explained what could have been done differently. This chapter is divided in several sections that includes possible improvement of the obtained results.

9.1 Constitutive model

Several methods can be used to study the interaction of foundations and soils. The known equation of motions proposed is valid in time domain and is considered for linear-elastic models. However, the appropriate soil constitutive model is more complex. Even with the most advanced soil model, a certain limitations are involved to simplify real soil behaviour [Liu et al., 2005]. A good consideration for determination of soil model is based on the characteristics of the problem. A linear-elastic soil model is easier to calibrate, but more assumptions have been made. In reality, vibrations causes a cyclic shear loading. A sequence of loading and unloading generates a hyseteric loop, which cannot be modelled with a linear-elastic model. Instead, a hardening soil small strain model is capable of this hyseteric loop, plasticity and in addition, it can describe hysteretic damping. Only such an advanced model requires more calibration factors to define the material properties. Appropriate behaviour of soils, i.e. plasticity-based analysis, can produce a substantiation modification which might lead to permanent increase of resulting vertical response [Amorosi & Boldini, 2009]. However, when using stiffer soils the advantage over simple models is little, as long as the soil is considered in very small strains [Fernández Ruiz & Medina Rodríguez, 2015].

9.2 Method

This study uses a three-dimensional finite element model. There are several other models which can be used to describe a soil intercation problem. A disadvantage of this finite element method is the required model size to describe the soil behaviour accurately. A more advanced method such as the boundary element method could have been used instead for the soil. This method has as advantage that it gives a suitable solution for dynamic problems in an unbounded domain [Birk & Behnke, 2012]. There are several methods to use the boundary element model, Genes [2012] has used a parallel coupled model based on finite

element method, boundary element method and scaled boundary finite element method. This has as advantage to models is time efficient for large-scale problems. However, this proposed model is made in two-dimensions. Andersen et al. [2007] has introduced a finite element and boundary element model to investigate moving loads representative for moving vehicles. Wherein a coupling between local finite elements with a boundary element model is described. Which solved the lack of ability of the finite element model to radiate energy at the boundaries.

Overall, the obtained results from the finite element method shows similarities with the result of Yu et al. [2013] study based on the dynamic Winkler model, and with Padrón et al. [2012] frequency domain coupled FE-BE model are similarities with a possibility to ommit the pile foundation for homogeneous cases. Based on the research of Deng et al. [2014] similarities were found, but in context of this study, the conclusion was different.

9.3 Parameter study

In the parameter study, a large amount of model configurations was tested; different homogeneous models, with and without piles, several layer configurations, also with and without piles, slenderness of piles, and influence of pulse loads. With these results a range of combinations could be described. However, suggested by Yu et al. [2013], the layer depth and material properties have stronger influence. This influence can be expressed with Equation 5.7 (p. 39). The tested layered models consists of only one combination of materials. Hence, it might have been relevant to slightly modify the relation between two different layers. Another method for obtaining results was described by Shahin [2016], which is based on artificial neural networks (ANN). This uses data for training and prediction. Only, this theory still has several shortcomings that needs further attention.

9.4 Foundation interaction

The interaction between foundations was tested in several cases (piles, slabs and combinations of those) at a specific frequency and only two cases (piles and slabs) for a whole range of frequencies. The two tested cases were representative for other options. However, there are many more other configurations what could have been investigated, such as cellars under a structure or the effect of grouped piles. Even the location of the source could change, instead of on a structure it might have a source in the soil, for example a tunnel.

Andersen [2014] has researched various structure combinations of building and subsoil. This have been done with the use of a coupled finite element and boundary element model. The source of the vibration is external and applied on the surface. It was obtained that the subsoil has strong influence on the building response. The inclusion of a cellar might change the ground floor displacement, whereas the strongest influence is obtained for layered soils.

Cellars defined as embedded basement of a structure could have influence on the response of the structure. Differences were observed by Turan et al. [2013], where the basement mass has a small influence on the motion at foundation base, but it has no influence on structure level. Only, small changes in mass or acceleration could influence the response significantly. Furthermore, an interesting behaviour of cellars can be the response due to interface and surface waves during harmonic loading.

Mentioned by Huang et al. [2016], the capacity and reliability of grouped piles versus single piles will increase, what might be beneficial in case of failure for a pile. However, a group of piles during harmonic vibration acts like one single pile, which is at lower frequencies observed by Gazetas et al. [1993], or a local pile-soil-pile interaction can be observed [Chow & Teh, 1991]. Furthermore, described by Caputo & Viggiani [1984], the interaction between two piles in groups remains linearly. It was also researched by Chow [1986] based on non-linear response the grouped pile-pile interaction remained elastic.

Wang et al. [2012] has studied the influence of vibration in a tunnel due to a high speed maglev train, and Guo et al. [2013] has introduced an underground subway station and introduced vibration on the surface. Both studies explains different approaches of the influence of a tunnel on the surrounding soil or at surface. Overall, the stratification of soil has influence on the vibration measured at the surface, whereas it tends that dry soil has a smaller vibration response than saturated soils. When introducing an vibration source at the soil, a tunnel cannot be ignored, since it results in an increased deformation of adjacent structures. However, mainly vibration with large wavelengths are affected by the presence of the tunnel compared to the shorter wavelengths.

Chapter 10

Reference Lists

Bibliography

J. Achenbach (1973). *Wave Propagation in Elastic Solids*. North-Holland Series in Applied Mathematics and Mechanics. Nort Holland.

A. Amorosi & D. Boldini (2009). 'Numerical modelling of the transverse dynamic behaviour of circular tunnels in clayey soils'. *Soil Dynamics and Earthquake Engineering* **29**(6):1059 – 1072.

L. Andersen (2006). *Linear Elastodynamic Analysis*. DCE Lecture Notes No. 3.

L. Andersen (2014). *Influence of dynamic soil-structure interaction on building response to ground vibration*, vol. 2, pp. 1087–1092. C R C Press LLC.

L. Andersen, et al. (2007). 'Numerical methods for analysis of structure and ground vibration from moving loads'. *Computers & Structures* **85**(1–2):43 – 58.

C. Birk & R. Behnke (2012). 'A modified scaled boundary finite element method for three-dimensional dynamic soil-structure interaction in layered soil'. *International Journal for Numerical Methods in Engineering* **89**(3):371–402.

R. Brinkgreve, et al. (2015a). 'Plaxis 3D AE Reference Manual'.

R. Brinkgreve, et al. (2015b). 'Plaxis 3D AE Scientific Manual'.

Y. Cai, et al. (2000). 'Nonlinear analysis of 3D seismic interaction of soil–pile–structure systems and application'. *Engineering Structures* **22**(2):191 – 199.

V. Caputo & C. Viggiani (1984). 'Pile foundation analysis: a simple approach to nonlinearity effects'. *Rivista Italiana di Geotecnica* **18**(2):32–51.

X. Chen, et al. (2015). 'Time-domain analysis of wave propagation in 3-D unbounded domains by the scaled boundary finite element method'. *Soil Dynamics and Earthquake Engineering* **75**:171 – 182.

Y. K. Chow (1986). 'Analysis of vertically loaded pile groups'. *International Journal for Numerical and Analytical Methods in Geomechanics* **10**(1):59–72.

Y. K. Chow & C. I. Teh (1991). 'Pile-Cap-Pile-Group Interaction in Nonhomogeneous Soil'. *Journal of Geotechnical Engineering* **117**(11):1655–1668.

R. D. Cook et al. (2007). *Concepts and applications of finite element analysis*. John Wiley & Sons.

G. Deng, et al. (2014). 'Soil-Pile Interaction in the Pile Vertical Vibration Based on Fictitious Soil-Pile Model'. *Journal of Applied Mathematics* **2014**.

C. Felippa (2004). 'A compendium of FEM integration rules for finite element work'. *Eng Comput* **21**:867–890.

J. Fernández Ruiz & L. Medina Rodríguez (2015). 'Application of an advanced soil constitutive model to the study of railway vibrations in tunnels through 2D numerical models: a real case in Madrid (Spain)'. *Revista de la construcción* **14**(3):55–63.

E. Flores-Mendez, et al. (2012). 'Rayleigh's, Stoneley's, and Scholte's interface waves in elastic models using a boundary element method'. *Journal of Applied Mathematics* **2012**.

G. Gazetas, et al. (1993). 'Dynamic response of pile groups with different configurations'. *Soil Dynamics and Earthquake Engineering* **12**(4):239–257.

M. C. Genes (2012). 'Dynamic analysis of large-scale {SSI} systems for layered unbounded media via a parallelized coupled finite-element/boundary-element/scaled boundary finite-element model'. *Engineering Analysis with Boundary Elements* **36**(5):845 – 857.

J. Guo, et al. (2013). 'Influence of a subway station on the inter-story drift ratio of adjacent surface structures'. *Tunnelling and Underground Space Technology* **35**:8 – 19.

T. H. Heaton (2005). *Engineering Seismology*. California Institute of Technology.

J. Huang, et al. (2016). 'Updating reliability of single piles and pile groups by load tests'. *Computers and Geotechnics* **73**:221 – 230.

S. L. Kramer (1996). *Geotechnical earthquake engineering*. Prentice Hall.

R. L. Kuhlemeyer & J. Lysmer (1973). 'Finite element method accuracy for wave propagation problems'. *Journal of Soil Mechanics & Foundations Div* **99**(Technical Report).

A. Laera & R. Brinkgreve (2015). 'PLAXIS Ground response analysis'. *Plaxis Bv* .

X. Liu, et al. (2005). 'Numerical modelling of nonlinear response of soil. Part 1: Constitutive model'. *International Journal of Solids and Structures* **42**(7):1849 – 1881.

G. Lombaert & G. Degrande (1999). 'Study of determining factors for traffic induced vibrations in buildings'. *Second biannual report BWM-1999-04, Department of Civil Engineering, Katholieke Universiteit Leuven* .

G. Lombaert, et al. (2001). 'The influence of the soil stratification on free field traffic-induced vibrations'. *Archive of Applied Mechanics* **71**(10):661–678.

A. E. H. Love (1929). 'The Stress Produced in a Semi-Infinite Solid by Pressure on Part of the Boundary'. *Philosophical Transactions of the Royal Society of London A: Mathematical, Physical and Engineering Sciences* **228**(659-669):377–420.

A. J. Lutenegger & D. J. D. Groot (1995). *Settlement of shallow foundations on granular soils.* Report. University of Massachusetts Transportation Center.

J. Lysmer & R. L. Kuhlemeyer (1969). 'Finite dynamic model for infinite media'. *Journal of the Engineering Mechanics Division* **95**(4):859–878.

N. M. Newmark (1959). 'A Method of Computation for Structural Dynamics'. *ASCE Journal of Engineering Mechanics Division* **85**(Technical Report).

S.-H. Ni, et al. (2011). 'Inclination correction of the parallel seismic test for pile length detection'. *Computers and Geotechnics* **38**(2):127 – 132.

T. Nogami & M. Novák (1976). 'Soil-pile interaction in vertical vibration'. *Earthquake Engineering & Structural Dynamics* **4**(3):277–293.

L. A. Padrón, et al. (2012). 'Simple superposition approach for dynamic analysis of piled embedded footings'. *International Journal for Numerical and Analytical Methods in Geomechanics* **36**(12):1523–1534.

O. Pal (1998). *Modélisation du comportement dynamique des ouvrages grâce à des éléments finis de haute précision.* Ph.D. thesis, thesis, L'université Joseph Fourier-Grenoble I.

A. V. Pichugin (2008). *Approximation of the Rayleigh wave speed.* Paper. University of Sheffield.

S. Plagenhoef (1992). 'The measurement of extremely low environmental frequencies'. *Neuroscience and Biobehavioral Reviews* **16**(4):473 – 480.

D. Ports & L. Zdravkovic (2001). 'Finite element analysis in Geotechnical engineering'.

D. Sahar & J. P. Narayan (2016). 'Quantification of modification of ground motion due to urbanization in a 3D basin using viscoelastic finite-difference modelling'. *Natural Hazards* **81**(2):779–806.

M. A. Shahin (2016). 'State-of-the-art review of some artificial intelligence applications in pile foundations'. *Geoscience Frontiers* **7**(1):33 – 44. Special Issue: Progress of Machine Learning in Geosciences.

A. Turan, et al. (2013). 'Seismic soil–structure interaction in buildings on stiff clay with embedded basement stories.'. *Canadian Geotechnical Journal* **50**(8):858 – 873.

United Nations, Department of Economic and Social Affairs (2015). *World Urbanization Prospects: The 2014 Revision, (ST/ESA/SER.A/366)*. Report. United Nations.

P. C. Vinh (2013). 'Scholte-wave velocity formulae'. *Wave Motion* **50**(2):180 – 190.

J. Wang, et al. (2012). 'High-speed maglev train-guideway–tunnel–soil modelling of ground vibration'. *Proceedings of the Institution of Mechanical Engineers, Part F: Journal of Rail and Rapid Transit* **226**(3):331–344.

J. Yu, et al. (2013). 'Effect of sediment on vertical dynamic impedance of rock-socketed pile with large diameter'. *Journal of Central South University* **20**(10):2856–2862.

O. C. Zienkiewicz & R. L. Taylor (2000). *The finite element method: solid mechanics*, vol. 2. Butterworth-heinemann.